

Efficiency of the Keplerian accretion in the braneworld Kerr–Newman spacetimes and mining instability of some naked singularity spacetimes

Martin Blaschke* and Zdeněk Stuchlík†

*Institute of Physics and Research Centre of Theoretical Physics and Astrophysics,
Faculty of Philosophy and Science, Silesian University in Opava,
Bezručovo nám. 13, CZ-746 01 Opava, Czech Republic*

We show that the braneworld rotating Kerr–Newman black hole and naked singularity spacetimes with both positive and negative braneworld tidal charge parameter can be separated into fourteen classes according to properties of circular geodesics governing the Keplerian accretion. We determine efficiency of the Keplerian accretion disks for all braneworld Kerr–Newman spacetimes. We demonstrate occurrence of an infinitely deep gravitational potential in Kerr–Newman naked singularity spacetimes having the braneworld dimensionless tidal charge $b \in (1/4, 1)$ and the dimensionless spin $a \in (2\sqrt{b} - \sqrt{b(4b-1)}, 2\sqrt{b} + \sqrt{b(4b-1)})$, implying unbound efficiency of the Keplerian accretion and possibility to extract the whole naked singularity mass. Therefore, we call them braneworld “mining-unstable” Kerr–Newman naked singularity spacetimes. Fundamental restriction on the relevance of the extraordinary but fully classical phenomenon of the mining instability is given by validity of the assumption of geodesic motion of the accreting matter.

PACS numbers: 11.25.Uv 04.70.Bw , 04.50.-h

Keywords: D branes; black hole, Keplerian accretion, infinite effectiveness, mining instability

I. INTRODUCTION

In recent years, one of the most interesting and promising approaches to the force-unification theory is represented by the higher-dimensional String theory and particularly M-theory [1, 2]. In the String and M-theory, gravity is described as a truly higher-dimensional interaction becoming effectively 4D at low enough energies. These theories inspired the so called braneworld models, in which the observable universe is a 3D-brane on which the standard particle-model fields are confined, while gravity enters the extra spatial dimensions [3]. The braneworld models provide an elegant solution to the hierarchy problem of the electroweak and quantum gravity scales, as these scales could become of the same order (TeV) due to the large scale extra dimensions [3]. In fact, gravity can be localized near the D3 brane in the bulk space with a non-compact, infinite size extra dimension with the warped spacetime satisfying the 5D Einstein equations [4] - the non-compact dimension can be related to the M-theory. Future collider experiments can test the braneworld models quite well, including even the hypothetical mini black hole production [5].

The 5D Einstein equations at the bulk space can be constrained to the 3D brane implying thus modified 4D Einstein equations [6]. Solution of these constrained 4D Einstein equations is quite complex in the presence of the matter stress energy tensor, e.g., in the case of models of neutron stars [7–9]. However, it can be relatively simple in the case of vacuum solutions related to braneworld black holes. For both, the spherically symmetric and

static black holes that can be described by the Reissner–Nordström geometry [10], and the axially symmetric and stationary rotating black holes that can be described by the Kerr–Newman geometry [11], the influence due to the tidal effects from the bulk is simply represented by a single parameter that is called tidal charge because of the similarity of the effective stress-energy tensor of the tidal effects of the bulk space and the stress-energy tensor of the electromagnetic field [10].

The rotating braneworld black hole spacetimes, and the related naked singularity spacetimes, are thus represented by the Kerr–Newman geometry, but without the associated electromagnetic field occurring in the standard general relativity [12]. The tidal charge parameter can be both positive and negative [10, 11], while in the standard general relativity only positive parameter corresponding to the square of the electric charge occurs.

The standard studies of the Reissner–Nordström or Kerr–Newman black hole and naked-singularity geodesic motion [13–17] can thus be directly applied for the braneworld black holes and naked singularities with positive tidal charge. The astrophysically relevant implications of the geodesic motion were extensively studied for the braneworld black holes (with both positive and negative tidal charges) in a number of papers related to the optical effects [18–25], or the test particle motion [26–33].

Here we study circular motion of test particles and photons in the braneworld Kerr–Newman spacetimes and give classification of the braneworld black hole and naked singularity spacetimes according to the properties of the radial profiles of specific angular momentum and specific energy of sequences of corotating and retrograde circular orbits. We give the classification for both the positive and negative values of the dimensionless tidal charge parameter. We also determine efficiency of the Keplerian

* martin.blaschke@fpf.slu.cz

† zdenek.stuchlik@fpf.slu.cz

accretion disks that is related to the astrophysically relevant accretion from infinity (large distance) downwards to the first limit on existence of stable circular geodesics.

A very detailed analysis of the circular motion of electrically neutral test particles in the standard Kerr–Newman spacetimes has been presented in [17], where both black hole and naked singularity spacetimes were discussed. The results of this study are relevant in the braneworld spacetimes with positive tidal charges; we do not repeat them, focusing our study to the phenomena related to the Keplerian accretion, its efficiency, and the phenomenon of a new special instability of the naked singularity spacetimes that were not considered in the paper [17]. Along with the standard classical instability due to the Keplerian accretion occurring in the Kerr naked singularity spacetimes, leading to their conversion to a Kerr black hole [34–37], we have found a special class of classical instability, called here “mining” instability, as

this instability is related to an unlimitedly deep gravitational potential well, occurring in the class of the Kerr–Newman naked singularity spacetimes with appropriately restricted values of their dimensionless spin a and dimensionless tidal charge b . We briefly discuss the limits on the applicability of the Keplerian accretion in relation to the mining instability.

II. BRANEWORLD KERR–NEWMAN GEOMETRY

Using the standard Boyer–Lindquist coordinates (t, r, θ, φ) and the geometric units ($c = G = 1$), we can write the line element of a rotating (Kerr–Newman) black hole or naked singularity, representing solution of the Einstein equations constrained to the 3D-brane, in the form [10, 11]

$$ds^2 = - \left(1 - \frac{2Mr - b}{\Sigma} \right) dt^2 - \frac{2a(2Mr - b)}{\Sigma} \sin^2 \theta dt d\varphi + \frac{\Sigma}{\Delta} dr^2 + \Sigma d\theta^2 + \left(r^2 + a^2 + \frac{2Mr - b}{\Sigma} a^2 \sin^2 \theta \right) \sin^2 \theta d\varphi^2, \quad (1)$$

where

$$\begin{aligned} \Delta &= r^2 - 2Mr + a^2 + b, \\ \Sigma &= r^2 + a^2 \cos^2 \theta. \end{aligned} \quad (2)$$

M is the mass parameter of the spacetime, $a = J/M$ is the specific angular momentum of the spacetime with internal angular momentum J , and the braneworld parameter b , called “tidal charge”, represents imprint of the non-local (tidal) gravitational effects of the bulk space [11].

The form of the metric (1) is the same as that of the standard Kerr–Newman solution of the 4D Einstein–Maxwell equations, with squared electric charge Q^2 being replaced by the tidal charge b [12]. We can separate three cases:

- a) $b = 0$ in which we are dealing with the standard Kerr metric.
- b) $b > 0$ in which we are dealing with the standard Kerr–Newman metric.
- c) $b < 0$ in which we are dealing with the non-standard Kerr–Newman metric.

Notice that in the braneworld Kerr–Newman spacetimes the geodesic structure is relevant also for the motion of electrically charged particles, as there is no electric charge related to these spacetimes. On the other hand, the case (b) can be equally considered for the analysis of the uncharged particle motion in the standard electrically charged Kerr–Newman spacetime.

For simplicity we put in the following considerations $M = 1$. Then the spacetime parameters a and b , and the time t and radial r coordinates become dimensionless. This is equivalent to the redefinition when we express all the quantities in units of M : $a/M \rightarrow a$, $b/M^2 \rightarrow b$, $t/M \rightarrow t$ and $r/M \rightarrow r$.

Separation between the black hole and naked singularity spacetimes is given by the relation of the spin and tidal charge parameters in the form

$$a^2 + b = 1 \quad (4)$$

determining the so called extreme black hole with coinciding horizons. The condition $0 < a^2 + b < 1$ governs black hole spacetimes with two distinct event horizons, while the condition $a^2 + b < 0$ governs black hole spacetimes with only one distinct event horizon at $r > 0$. For $a^2 + b > 1$, the spacetime describes a naked singularity.

For positive tidal charges the black hole spin has to be $a^2 < 1$, as in the standard Kerr–Newman spacetimes, but for negative tidal charges there can exist black holes violating the well know Kerr limit, having $a^2 > 1$ [28].

Using substitutions

$$dt = dx^0 + \left(\frac{r^2 + a^2}{\Delta} - 1 \right) dr, \quad (5)$$

$$d\varphi = d\tilde{\varphi} + \frac{a}{\Delta} dr, \quad (6)$$

$$x = (r \cos(\tilde{\varphi}) + a \sin(\tilde{\varphi})) \sin \theta, \quad (7)$$

$$y = (r \sin(\tilde{\varphi}) - a \cos(\tilde{\varphi})) \sin \theta, \quad (8)$$

$$z = r \cos \theta, \quad (9)$$

the braneworld Kerr–Newman geometry can be transformed into the so called Kerr–Schild form using the Cartesian coordinates:

$$ds^2 = -(dx^0)^2 + (dx)^2 + (dy)^2 + (dz)^2 + \frac{(2Mr - b)r^2}{r^4 + a^2z^2} \left\{ dx^0 - \frac{1}{r^2 + a^2} \left[r(xdx + ydy) + a(xdy - ydx) - \frac{1}{r}zdz \right] \right\}^2, \quad (10)$$

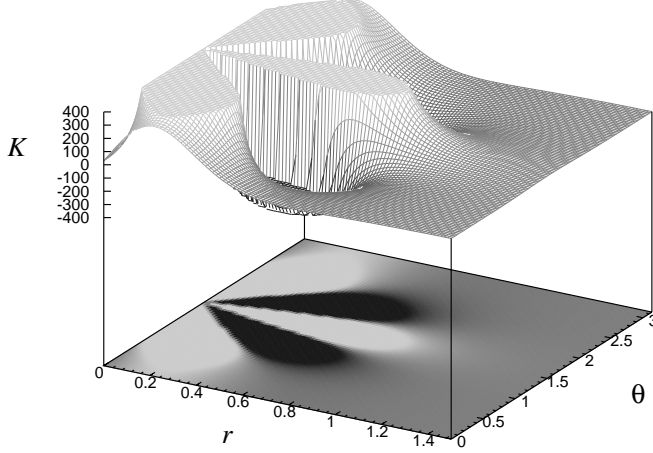


FIG. 1. Example of the behaviour of Kretschmann's scalar K for $a = 0.8$ and $b = -0.8$ to illustrate its similarity to Kerr–Newman case.

where r is defined, implicitly, by

$$r^4 - r^2(x^2 + y^2 + z^2 - a^2) - a^2z^2 = 0.$$

A. Singularity

The metric (10) is analytical everywhere except at points satisfying the condition

$$x^2 + y^2 + z^2 = a^2 \quad \text{and} \quad z = 0. \quad (11)$$

This condition is the same as in the case of the Kerr black holes or naked singularities, so we clearly see that the braneworld parameter b has no influence on the position of the physical singularity of the space-time. The physical “ring” singularity of the braneworld rotating black holes (and naked singularities) is located at $r = 0$ and $\theta = \pi/2$, as in the Kerr spacetimes.

We describe the influence of the braneworld tidal charge parameter b on the Kerr-like ring singularity at $r = 0, \theta = \pi/2$ using the Kretschmann scalar $K = R_{\alpha\beta\gamma\delta}R^{\alpha\beta\gamma\delta}$ representing an appropriate tool to probe the structure of spacetimes singularities. Using (1) we obtain

$$K = \frac{8}{(r^2 + a^2y^2)^6} (r^4A - 2a^2r^2By^2 + a^4Cy^4 - 6a^6M^2y^6), \quad (12)$$

where

$$y = \cos \theta, \quad (13)$$

$$A = (7b^2 - 12bMr + 6M^2r^2), \quad (14)$$

$$B = (17b^2 - 60bMr + 45M^2r^2), \quad (15)$$

$$C = (7b^2 - 60bMr + 90M^2r^2). \quad (16)$$

The Kretschmann scalar is formally the same as in the case of the Kerr–Newman metric with $Q^2 \rightarrow b$ [38]. Naturally, the negative values of brane parameter would have some effect onto K , but as we can see from denominator of (12), it does not influence the location of the singularity. As an example we demonstrate behaviour of the scalar K for $a = 0.8$ and $b = -0.8$ near the ring singularity in the Figure (1).

For completeness we give also the Ricci tensor whose

components take the form:

$$R_{tt} = 4b \frac{a^2 + 2\Delta - a^2 \cos(2\theta)}{(a^2 + 2r^2 + a^2 \cos(2\theta))^3}, \quad (17)$$

$$R_{t\varphi} = -8ab \frac{(a^2 + \Delta) \sin^2 \theta}{(a^2 + 2r^2 + a^2 \cos(2\theta))^3}, \quad (18)$$

$$R_{\varphi t} = R_{t\varphi}, \quad R_{rr} = -\frac{R_{\theta\theta}}{\Delta}, \quad (19)$$

$$R_{\theta\theta} = \frac{2b}{a^2 + 2r^2 + a^2 \cos(2\theta)}, \quad (20)$$

$$R_{\varphi\varphi} = 4b \sin^2(\theta) \frac{3a^4 + 2r^4 + a^2(b - 2Mr + 5r^2)}{(a^2 + 2r^2 + a^2 \cos(2\theta))^3} \quad (21)$$

$$- \frac{a^2 \Delta \cos(2\theta)}{(a^2 + 2r^2 + a^2 \cos(2\theta))^3}. \quad (22)$$

Ricci scalar is zero automatically by construction of the braneworld Kerr–Newman solution [10].

B. Ergosphere

Here we demonstrate influence of the braneworld tidal charge parameter b on the ergosphere whose boundary is defined by the condition:

$$g_{tt} = r^2 - 2Mr + a^2 \cos^2 \theta + b = 0. \quad (23)$$

Extension of the ergosphere in the latitudinal coordinate θ is determined by the maximal latitude given by the relation

$$\cos^2 \theta_{\max} = \frac{1 - b}{a^2}. \quad (24)$$

We can see that existence of the ergosphere is limited by the condition

$$b < 1. \quad (25)$$

We can infer that the ergosphere extension increases as the tidal charge parameter b decreases.

It is convenient to represent location of the ergosphere in the Kerr–Schild coordinates (10). Using the spacetime symmetry we can focus only on the polar slices with $y = 0$. In this case the condition for the static limit surface governing the border of the ergosphere is simply given by [39]

$$\begin{aligned} x^2 &= \frac{(a^2 + r^2) \Delta}{a^2}, \\ z^2 &= \frac{(2r - b)r^2 - r^4}{a^2}. \end{aligned} \quad (26)$$

In Figure (2) we illustrate influence of the braneworld tidal charge b on the ergosphere extension.

The ergosphere does not always completely surrounds the ring singularity. To illustrate this phenomenon, we give also dependence of the maximal allowed latitudinal

angle of the ergosphere on the dimensionless spin and dimensionless tidal charge.

For $b < 1$, the ergosphere exists for each dimensionless spin $a > 0$, covering all values of the latitudinal angle for the Kerr–Newman black holes. However, as the spin a increases for the Kerr–Newman naked singularities, the ergosphere extension shrinks – the maximal angle α decreases.

C. Causality violation region

In the “causality violation region” (sometimes called time-machine region) the axial coordinate φ takes time-like character implying possible existence of closed time-like curves. The causality violation region is defined by the condition

$$g_{\varphi\varphi} < 0. \quad (27)$$

In the equatorial plane the boundary of the causality violation region is determined by the condition

$$r^4 + a^2(r^2 + 2r - b) = 0. \quad (28)$$

The boundary of the causality violation region can be expressed by the relation

$$b = b_{\text{CV}} \equiv \frac{r(2a^2 + a^2 r + r^3)}{a^2}. \quad (29)$$

At Figure (3) we give some examples of the extension of the causality violation region. We see that for this region to exist above the ring singularity, the tidal charge has to be positive. With increasing values of the parameters $b > 0$ and a , the causality violation region expands.

The equation (28) gives us maximal possible extension of causal violation region located at

$$r_{\text{Max}} = \sqrt{1 + b} - 1. \quad (30)$$

For positive b the value of r_{Max} is less than b and therefore, as we shall see later, the causality violation region cannot reach the region where the circular geodesics exist.

In the Kerr–Schild coordinates the boundary of the causality violation region is given by the relations

$$x^2 = \frac{(a^2 + r^2)^3}{a^2 \Delta}, \quad (31)$$

$$z^2 = \frac{r^2(a^2(b - 2r - r^2) - r^4)}{a^2 \Delta} \quad (32)$$

It can be proved that the causality violation region never overlaps with ergosphere and its extension is influenced by the braneworld parameter b in an opposite way. While causality violation region increases with increasing b , the ergosphere extension is getting smaller. This phenomenon is illustrated in Figure (2) where the Kerr–Schild coordinates are used.

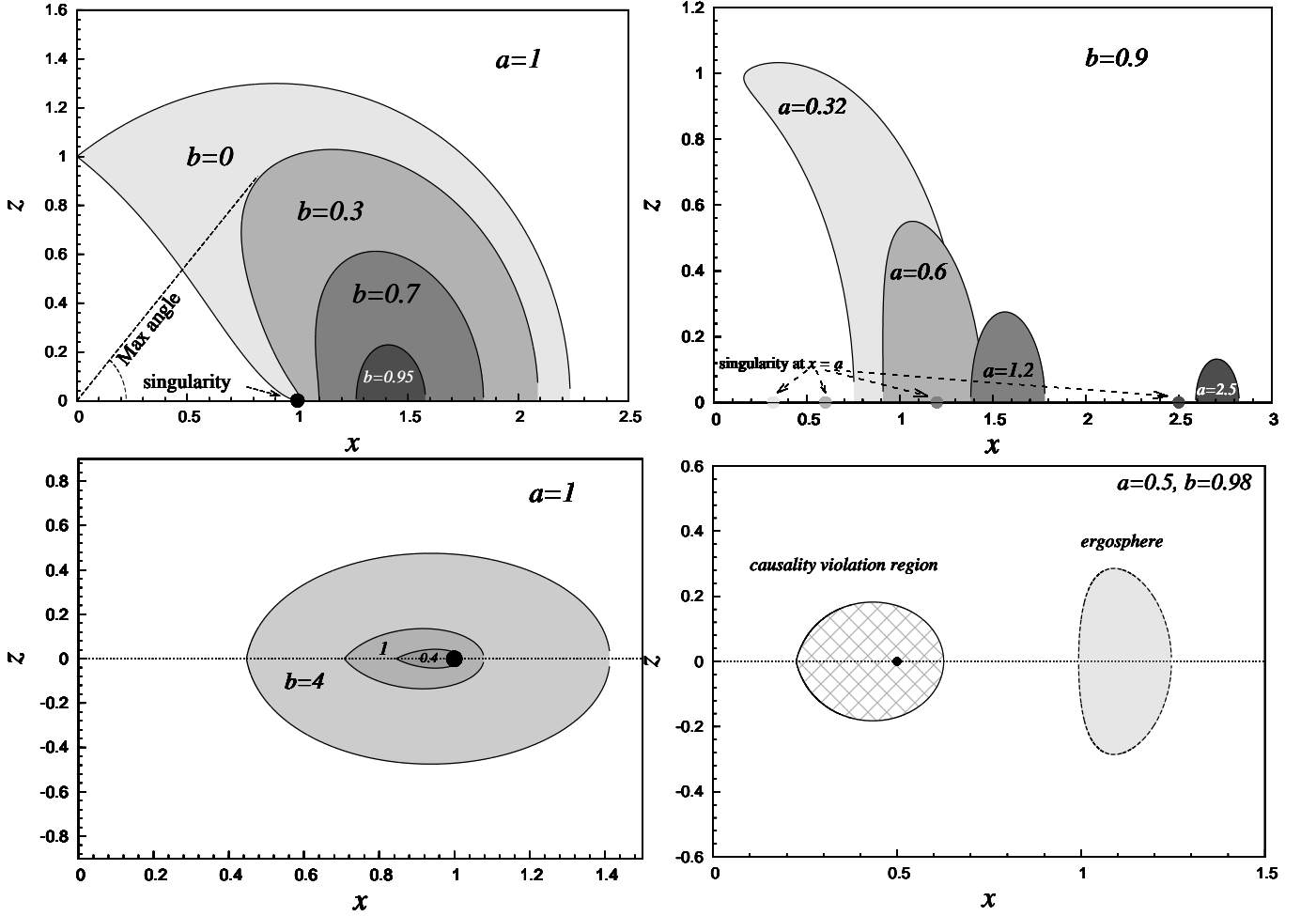


FIG. 2. **Upper Left:** Polar slice through the braneworld Kerr–Newman spacetime in the Cartesian KerrSchild coordinates. Dimensionless spin parameter a is fixed to value 1 and the braneworld parameter b is appropriately chosen to demonstrate its influence on the ergosphere. **Upper Right:** Polar slice through the braneworld Kerr–Newman spacetime in the Cartesian KerrSchild coordinates. The braneworld parameter b is fixed to value 0.9 and the spin parameter a is appropriately chosen to demonstrate its influence on the ergosphere. **Lower Left:** Causality violation region. **Lower Right:** Ergosphere and causality violation region.

In the following, we consider geodesic motion only in the regions above the causality violation region. For astrophysical phenomena occurring in the naked singularity spacetimes, it is usually assumed that above the boundary of the causality violation region the Kerr or Kerr–Newman spacetime is removed and substituted by different solution that could be inspired by the String theory – such objects are called superspinars [40–42]. Therefore, it is quite natural to assume that in the braneworld model framework, the inner boundary of the superspinars is located at radii larger than those related to the boundary of the causality violation region.

D. Locally non-rotating frames

In the rotating Kerr–Newman spacetimes physical processes can be most conveniently expressed in the family of locally non-rotating frames (LNRF), corresponding to zero angular momentum observers (ZAMO), with tetrad vectors given by the relations [43]

$$\mathbf{e}^{(t)} = (\omega^2 g_{\varphi\varphi} - g_{tt})^{\frac{1}{2}} \mathbf{dt}, \quad (33)$$

$$\mathbf{e}^{(\varphi)} = (g_{\varphi\varphi})^{\frac{1}{2}} (\mathbf{d}\varphi - \omega \mathbf{dt}), \quad (34)$$

$$\mathbf{e}^{(r)} = \left(\frac{\Sigma}{\Delta} \right)^{\frac{1}{2}} \mathbf{dr}, \quad (35)$$

$$\mathbf{e}^{(\theta)} = \Sigma^{\frac{1}{2}} \mathbf{d}\theta, \quad (36)$$

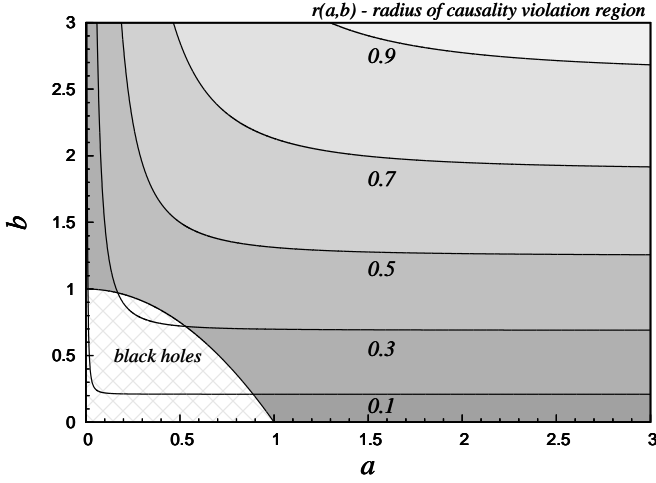


FIG. 3. Contour plot for radii of boundary of the causality violation region in the equatorial plane.

where ω is the angular velocity of the LNRF relative to distant observers and reads

$$\omega = -\frac{g_{t\varphi}}{g_{\varphi\varphi}} = \frac{a(2r-b)}{\Sigma(r^2+a^2) + (2r-b)a^2\sin^2\theta}. \quad (37)$$

Convenience of the LNRF can be demonstrated, e.g., in the case of the free fall of particles from infinity, which is purely radial only if related to the family of LNRFs [44].

E. Geodesic motion and Carter's equations

Using the Hamilton-Jacobi method, Carter found separated first order differential equations of the geodesic motion [39, 45], which in the case of the braneworld Kerr spacetimes take the form

$$\Sigma \frac{dr}{dw} = \pm \sqrt{R(r)}, \quad (38)$$

$$\Sigma \frac{d\theta}{dw} = \pm \sqrt{W(\theta)}, \quad (39)$$

$$\Sigma \frac{d\varphi}{dw} = -\frac{P_W}{\sin^2\theta} + \frac{aP_R}{\Delta}, \quad (40)$$

$$\Sigma \frac{dt}{dw} = -aP_W + \frac{(r^2+a^2)P_R}{\Delta}, \quad (41)$$

where

$$R(r) = P_R^2 - \Delta(m^2r^2 + \tilde{K}), \quad (42)$$

$$W(\theta) = (\tilde{K} - a^2m^2\cos^2\theta) - \left(\frac{P_w}{\sin\theta}\right)^2, \quad (43)$$

$$P_R(r) = \tilde{E}(r^2+a^2) - a\tilde{\Phi}, \quad (44)$$

$$P_W(\theta) = a\tilde{E}\sin^2\theta - \tilde{\Phi}. \quad (45)$$

Along with the conservative rest energy m , three constants of motion related to the spacetime symmetries has been introduced: \tilde{E} is the energy (related to the time Killing vector field), $\tilde{\Phi}$ is the axial angular momentum (related to the axial Killing vector field) and \tilde{K} is the constant of motion related to total angular momentum (related to the Killing tensor field) that is usually replaced by the constant $\tilde{Q} = \tilde{K} - (a\tilde{E} - \tilde{\Phi})^2$, since for the motion in the equatorial plane ($\theta = \pi/2$) there is $\tilde{Q} = 0$.

Note that the separable Eqs (38)-(41) are guaranteed in the Petrov type D spacetimes, in particular when the metric in the Boyer-Lindquist coordinates can be expressed in the Kerr-like form by replacing the mass parameter M by a function $M(r)$ independent of latitude θ . In the braneworld rotating black hole spacetimes there is $M(r) = M - \frac{b}{2r}$. Generally, these equations can be integrated and expressed in terms of the hyper-elliptic integrals [12, 46, 47]. The Carter equations can be also generalized to the motion in the Kerr-Newman-de Sitter spacetimes [39, 46, 48-50].

For the geodesic motion of photons, we put $m = 0$ in the Carter equations. Analysis of the photon motion in the standard Kerr-Newman spacetimes [17, 51, 52] can be directly applied to the case of photon motion in the braneworld Kerr-Newman spacetimes. It has been done in [19, 53]; we use results of these works in the following discussions.

We have to construct classification of the braneworld Kerr-Newman spacetimes according to the properties of circular geodesics governing the Keplerian accretion that can be related not only to the standard accretion discs, but also to the quasicircular motion of gravitationally radiating particles. We give classification according to properties of the circular null geodesics and stability of the circular geodesics that is the critical attribute of the Keplerian accretion. Finally, we combine the effects given by these two classifications. Of course, we have to include into the classification as relevant criteria also existence of the event horizons and existence of the ergosphere.

III. CIRCULAR GEODESIC MOTION

In general stationary and axially symmetric spacetime with the Boyer-Lindquist coordinate system (t, r, θ, φ) and $(-+++)$ signature of the metric tensor, the line element is given by

$$ds^2 = g_{tt}dt^2 + 2g_{t\varphi}dtd\varphi + g_{rr}dr^2 + g_{\theta\theta}d\theta^2 + g_{\varphi\varphi}d\varphi^2. \quad (46)$$

The metric (46) is adapted to the symmetries of the spacetime, endowed with the Killing vectors $(\partial/\partial t)$ and $(\partial/\partial\varphi)$ for time translations and spatial rotations, respectively. For geodesic motion in the equatorial plane ($\theta = \pi/2$), the metric functions g_{tt} , $g_{t\varphi}$, g_{rr} , $g_{\theta\theta}$ and $g_{\varphi\varphi}$ in Eq. (46) depend only on the radial coordinate r . So except the rest energy m , two integrals of the motion are

relevant as $\tilde{Q} = 0$:

$$U_t = -E, \quad U_\varphi = L, \quad (47)$$

where the 4-velocity $U_\alpha = g_{\alpha\nu} dx^\nu/d\tau$, with τ being the affine parameter. In the case of asymptotically flat spacetime, we can identify at infinity the motion constant $E = \tilde{E}/m$ as the specific energy, i.e., energy related to the rest energy, and the motion constant $L = \tilde{\Phi}/m$ as the specific angular momentum.

The geodesic equations of the equatorial motion take the form (see, e.g., [54])

$$\frac{dt}{d\tau} = \frac{Eg_{\varphi\varphi} + Lg_{t\varphi}}{g_{t\varphi}^2 - g_{tt}g_{\varphi\varphi}}, \quad \frac{d\varphi}{d\tau} = -\frac{Eg_{t\varphi} + Lg_{tt}}{g_{t\varphi}^2 - g_{tt}g_{\varphi\varphi}}, \quad (48)$$

and

$$g_{rr} \left(\frac{dr}{d\tau} \right)^2 = R(r), \quad (49)$$

where the radial function $R(r)$ is defined by

$$R(r) \equiv -1 + \frac{E^2 g_{\varphi\varphi} + 2ELg_{t\varphi} + L^2 g_{tt}}{g_{t\varphi}^2 - g_{tt}g_{\varphi\varphi}}. \quad (50)$$

A. Energy, angular momentum and angular velocity of circular geodesics

For circular geodesics in the equatorial plane, the conditions

$$R(r) = 0 \quad \text{and} \quad \partial_r R(r) = 0 \quad (51)$$

must be satisfied simultaneously. These conditions determine the specific energy E , the specific angular momentum L and the angular velocity $\Omega = d\varphi/dt$ related to distant observers, for test particles following the circular geodesics, as functions of the radius and the spacetime parameters in the form

$$E = \pm \frac{g_{tt} + g_{t\varphi}\Omega}{\sqrt{-(g_{tt} + 2g_{t\varphi}\Omega + g_{\varphi\varphi}\Omega^2)}}, \quad (52)$$

$$L = \mp \frac{g_{t\varphi} + g_{\varphi\varphi}\Omega}{\sqrt{-(g_{tt} + 2g_{t\varphi}\Omega + g_{\varphi\varphi}\Omega^2)}}, \quad (53)$$

$$\Omega = \frac{-g_{t\varphi,r} \pm \sqrt{(g_{t\varphi,r})^2 - g_{tt,r}g_{\varphi\varphi,r}}}{g_{\varphi\varphi,r}}, \quad (54)$$

where the upper and lower signs refer to two families of solutions. To avoid any misunderstanding, we will refer to these two families as the upper sign family, and the lower sign family. At large distances in the asymptotically flat spacetimes, the upper family orbits are corotating, while the lower family orbits are counterrotating with respect to rotation of the spacetime. This separation holds in the whole region above the event horizon of the Kerr–Newman black hole spacetimes, but it is not

necessarily so in all the Kerr–Newman naked singularity spacetimes – in some of them the upper family orbits become counterrotating close to the naked singularity as demonstrated in [35].

Using the spacetime line element of the braneworld rotating spacetimes given by (1) [11, 55], with the assumption of $M = 1$, we obtain the radial profiles of the specific energy, specific axial angular momentum and the angular velocity related to infinity of the circular geodesics in the form:

$$E = \frac{r^2 - 2r + b \pm a\sqrt{r-b}}{r\sqrt{r^2 - 3r + 2b \pm 2a\sqrt{r-b}}}, \quad (55)$$

$$L = \pm \frac{\sqrt{r-b}(r^2 + a^2 \mp 2a\sqrt{r-b}) \mp ab}{r\sqrt{r^2 - 3r + 2b \pm 2a\sqrt{r-b}}}, \quad (56)$$

$$\Omega = \pm \frac{1}{\frac{r^2}{\sqrt{r-b}} \pm a}. \quad (57)$$

From equations (55)–(57) we immediately see that two restrictions on the existence of circular geodesics have to be satisfied:

$$r^2 - 3r + 2b \pm 2a\sqrt{r-b} \geq 0, \quad (58)$$

$$r \geq b. \quad (59)$$

The equality in the first condition determines the photon circular geodesics – this demonstrates that positions of circular orbits of test particles are limited by the circular geodesics of massless particles. The second, reality condition is relevant in the Kerr–Newman spacetimes with positive tidal charge b only, if we restrict attention to the region of positive radii.

B. Effective potential

Instead of the radial function $R(r, a, b, E, L)$, the equatorial motion of test particles can be conveniently treated by using the so called effective potential $V_{\text{eff}}(r, a, b, L)$ that is related to the particle specific energy and depends on the specific angular momentum of the motion and the spacetime parameters. The equation $E = V_{\text{eff}}$ determines the turning points of the radial motion of the test particle.

The notion of the effective potential is useful in treating the Keplerian (quasigeodesic) accretion onto the central object that is directly related to the circular geodesic motion [56, 57]. The circular geodesics are governed by the local extrema of the effective potential; the accretion process is possible in the regions of stable circular geodesics corresponding to the local minima of the effective potential.

The effective potential can be easily derived using the normalization condition for the test particle motion

$$U_\alpha U^\alpha = -1 \quad (60)$$

that implies for the equatorial motion relation

$$g_{rr} \left(\frac{dr}{d\tau} \right)^2 = (E - V_{\text{Eff}+})(E - V_{\text{Eff}-}), \quad (61)$$

and in the general stationary and axisymmetric space-times the effective potential can be expressed in the form

$$V_{\text{Eff}\pm}(r, a, b, L) = \frac{\beta \pm \sqrt{\beta^2 - \alpha\gamma}}{\alpha}, \quad (62)$$

where

$$\alpha = \frac{g_{\varphi\varphi}}{g_{\varphi t}^2 - g_{\varphi\varphi}g_{tt}}, \quad \beta = \frac{-Lg_{t\varphi}}{g_{\varphi t}^2 - g_{\varphi\varphi}g_{tt}}, \quad (63)$$

$$\gamma = \frac{L^2g_{tt}}{g_{\varphi t}^2 - g_{\varphi\varphi}g_{tt}} - 1. \quad (64)$$

This form can be simplified into

$$V_{\text{Eff}\pm} = \frac{-Lg_{t\varphi} \pm \sqrt{(L^2 + g_{\varphi\varphi})(g_{\varphi t}^2 - g_{\varphi\varphi}g_{tt})}}{g_{\varphi\varphi}}. \quad (65)$$

For massless particles, $m = 0$, we formally obtain

$$\frac{V_{\text{EffP}}(r, a, b)}{L} = \frac{a(2r - b) \pm r^2\sqrt{\Delta}}{r^4 + a^2(r^2 + 2r - b)}. \quad (68)$$

Here the $+$ sign is valid if $L > 0$ and the $-$ sign is valid if $L < 0$. Of course, we know that the photon geodesic motion is independent of the photon energy, being dependent of the impact parameter $l = L/E$ for the equatorial motion [41, 59].

The effective potential is symmetric under transformation $a \rightarrow -a, L \rightarrow -L$, therefore, we will only study the Kerr–Newman braneworld spacetimes with non-negative values of the spin parameter a .

The effective potential has a discontinuity (divergence) at radii determined by the conditions:

$$g_{\varphi t}^2 - g_{\varphi\varphi}g_{tt} = 0, \quad (69)$$

$$r^4 + a^2(r^2 + 2r - b) = 0. \quad (70)$$

At the equatorial plane, the quantity $g_{\varphi t}^2 - g_{\varphi\varphi}g_{tt} \equiv \Delta$, and the condition (69) implies that the effective potential diverges at the event horizons. The second condition (70) for possible divergence of the effective potential can be transformed to the relation

$$b = b_s \equiv \frac{r(2a^2 + a^2r + r^3)}{a^2}. \quad (71)$$

Notice that the functions $b_s(r, a)$ and $b_{\text{CV}}(r, a)$ are equivalent – therefore, the divergence could occur just

We have to choose the upper (plus) sign of the general expression of the effective potential, as this case represents the boundary of the motion of particles in the so called positive root states having positive locally measured energy and future-oriented time component of 4-velocity. The lower (minus) sign expression of the effective potential is irrelevant here, as it determines in the regions of interest particles in the so called negative-root states having negative locally measured energy and past-oriented time component of the 4-velocity, being thus related to the Dirac particles – for details see [12, 58].

The physically relevant condition of the test particle motion reads

$$E \geq V_{\text{Eff}+}. \quad (66)$$

For particles with the non-zero rest mass, $m > 0$, the explicit form of the effective potential in the braneworld Kerr–Newman spacetimes reads

$$V_{\text{Eff}}(r, a, b, L) = \frac{aL(2r - b) + r\sqrt{\Delta}\sqrt{L^2r^2 + r^4 + a^2(r^2 + 2r - b)}}{r^4 + a^2(r^2 + 2r - b)}. \quad (67)$$

at the boundary of the causality violation region. In the limit of $b \rightarrow b_s$, the numerator of (67) reads

$$-\frac{r}{a}(L - |L|)(a^2 + r^3). \quad (72)$$

Thus if $L \geq 0$, both numerator and denominator of (67) are zero and we have to use the L'Hopital rule to obtain

$$\lim_{b \rightarrow b_s} V_{\text{Eff}} = \begin{cases} \frac{r^4 + a^4 + 2a^2(L^2 + r^2) + L^2r^2}{2aL(a^2 + r^2)} & L \geq 0 \\ \infty & L < 0 \end{cases}, \quad (73)$$

Therefore, for the specific angular momentum $L < 0$ the effective potential approaches at the discontinuity the positive infinity, creating thus for the test particles with $L < 0$ an impenetrable barrier. On the other hand, for particles with $L \geq 0$, the effective potential takes at the boundary of the causality violation region a finite value that depends on the specific angular momentum.

The last square root in equation (67) is negative for

$$b > \frac{r(2a^2 + a^2r + L^2r + r^3)}{a^2}, \quad (74)$$

therefore the effective potential can be undefined for small values of r . However, this could happen only in the causality violation region where the effective potential loses its relevance because of the modified meaning of the axial coordinate that has time-like character in this region.

C. Energy measured in LNRF

It is useful to determine for particles on the circular geodesics the locally measured energy, related to some properly defined family of observers. The specific energy related to the LNRF (E_{LNRF}) is given by the projection of the 4-velocity on the time-like vector of the frame:

$$E_{\text{LNRF}} = U^{(t)} = U^\mu \mathbf{e}_\mu^{(t)} = \left(\frac{dt}{d\tau} \right) \mathbf{e}_t^{(t)} \quad (75)$$

$$= \frac{r^2 \pm a\sqrt{r-b}}{\sqrt{r^4 + a^2(r^2 + 2r - b)}} \frac{\sqrt{\Delta}}{\sqrt{r^2 - 3r + 2b \pm 2a\sqrt{r-b}}}.$$

The locally measured particle energy must be always positive for the particles in the positive-root states assumed here – while it is negative for the negative-root states that are physically irrelevant in the context of our study [58].

The LNRF energy of particle following the circular geodesics diverges on the photon circular orbit as well as the covariant energy E . It also diverges for circular orbits approaching the boundary of the causality violation region given by equation (70).

D. Future-oriented particle motion

For the positive-root states the time evolution vector has to be oriented to future, i.e., $dt/d\tau > 0$. On the other hand, the negative-root states have past oriented time vectors, $dt/d\tau < 0$, being thus physically irrelevant for our study. To be sure that we are using the solutions related to the proper effective potential V_{eff} with the correct upper sign, we have to check that the considered geodesics have proper orientation $dt/d\tau > 0$.

Using the metric (1) and relations for the specific energy (55) and specific angular momentum (56) in equation (48), we obtain the time component of the 4-velocity for both the upper and lower family circular geodesics in the form

$$\frac{dt}{d\tau} = \frac{r^2 \pm a\sqrt{r-b}}{r\sqrt{r^2 - 3Mr + 2b \pm 2a\sqrt{Mr-b}}}. \quad (76)$$

We see from this equation that the time component is always positive for both the orbits of the upper and lower family, so we always have the positive-root states and no mixing with the negative-roots states occurs.

IV. CIRCULAR GEODESICS OF PHOTONS

We first study motion of photons, as the photon circular orbits represent a natural boundary for existence of

$b \backslash r$	$(-\infty; 0)$	$(0; \frac{3}{4})$	$(\frac{3}{4}; 1)$	1	$(1; \frac{9}{8})$	$(\frac{9}{8}; \infty)$	$a_{\text{ph}}(r, b)$
1	max	max	min	–	–	–	$\sqrt{1-b}$
r_1, r_2	min	min	min	min	min	–	0
$\frac{4}{3}b$	–	min	max	max	max	min	$\frac{\sqrt{b}}{3\sqrt{3}}(8b-9)$
a_{phMin}	$-b$	∞	∞	0	∞	∞	–

TABLE I. All kinds of extrema of function $a_{\text{ph}}(r, b)$. We show the (+) sign part only because of the symmetry corresponding to interchangeability between signs (\pm) and nature of local minima (max/min). Function a_{phMin} is value of function $a_{\text{ph}}(r, b)$ at lowest possible r , which is $r = 0$ for non-positive values of b and $r = b$ otherwise.

the circular geodesic motion [52, 59].

The general photon motion in the braneworld Kerr–Newman black hole spacetimes was studied in [19]. Here we concentrate on the equatorial photon motion and especially on the existence of the photon circular orbits. In case of the equatorial photon orbits, the radial function $R(r)$ is determined by the equation (50) with removed term -1 (as the rest energy $m = 0$) that can be transformed into the form [19]:

$$\frac{R}{E^2} = \frac{[r^2 - a(\lambda - a)]^2 - \Delta(\lambda - a)^2}{r^2 \Delta}, \quad (77)$$

where the impact parameter λ is defined by the relation

$$\lambda = \frac{L}{E}. \quad (78)$$

Notice that photon orbits depend only on the impact parameter λ .

Applying conditions for the circular motion (51), we find that the equatorial photon circular orbits are given by the equations

$$[r^2 - a(\lambda - a)]^2 - \Delta(\lambda - a)^2 = 0, \quad (79)$$

$$2r(r^2 + a^2 - a\lambda) - (r - 1)(\lambda - a)^2 = 0. \quad (80)$$

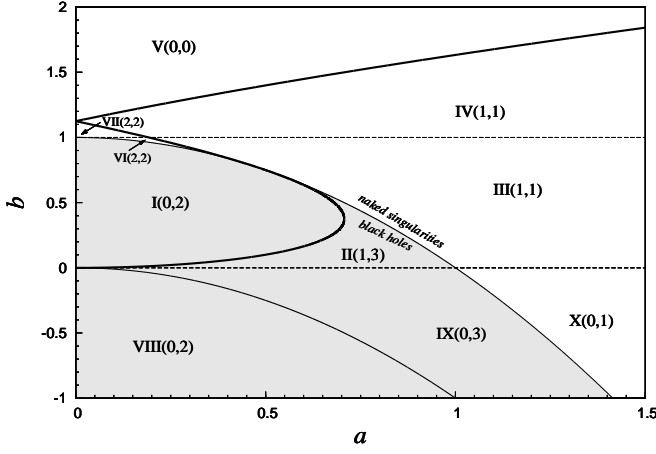


FIG. 4. Braneworld Kerr–Newman black holes and naked singularities can be divided into ten distinguish classes according to the properties of circular photon geodesics. Curve $a_{\text{ph}}(4b/3, b)$ (full line), given by (88), plays the main role in the classification. The corresponding regions of b - a plane are denoted by I–X; the numbers in brackets denote the number of the circular photon orbits in the respective class. The first number determines number of the stable circular photon geodesics, the second number determines number of the unstable circular photon geodesics.

These two conditions imply that the radii of circular photon orbits are determined by equation

$$r^2 - 3r + 2a^2 + 2b \pm 2a\sqrt{\Delta} = 0, \quad (81)$$

and the impact parameter λ is given by the equation

$$\lambda = -a \frac{r^2 + 3r - 2b}{r^2 - 3r + 2b}. \quad (82)$$

Furthermore, the equation (81) can be transformed into the form

$$r^2 - 3r + 2b \pm 2a\sqrt{r-b} = 0 \quad (83)$$

that implies the same reality condition on the radius of the photon orbit r_{ph} as the one that follows from equations (55)–(57):

$$r_{\text{ph}} \geq b. \quad (84)$$

Due to the reality condition the numerator in equation (82) is positive, while the (\pm) sign of the denominator is determined by the sign in equation (83). Thus we obtain corotating orbits ($\lambda > 0$) for the upper sign in (83) and counterrotating orbits ($\lambda < 0$) in the other case.

The solution of the equation (83) can be expressed in the form

$$a = a_{\text{ph}}(r, b) \equiv \pm \frac{(3r - r^2 - 2b)}{2\sqrt{r-b}}. \quad (85)$$

For given a and b the points of a line $a = \text{const}$ crossing the function $a_{\text{ph}}(r, b)$ determine radius r_{ph} of the photon

circular orbits. We restrict our discussion to the solutions corresponding to $a > 0$, giving both corotating and counterrotating orbits. The zeros of the function $a_{\text{ph}}(r, b)$ are located at

$$r_{\text{ph}\pm} = \frac{1}{2} \left(3 \pm \sqrt{9 - 8b} \right). \quad (86)$$

Note that these solutions represent radii of photon circular orbits in the Reissner–Nordström spacetimes [15, 16]. Since

$$\frac{\partial a_{\text{ph}}}{\partial r} = \pm \frac{(r-1)(3r-4b)}{4(r-b)^{3/2}}, \quad (87)$$

the extrema of the curves $a_{\text{ph}}(r, b)$ are located at $r = 1$ and at $r = 4b/3$. The value of the function $a_{\text{ph}}(r, b)$ at the point $r = 1$ reads (recall that we consider the positive values of spin)

$$a_{\text{ph-ex}}(r = 1, b) = \sqrt{1-b}, \quad (88)$$

corresponding to the extreme Kerr–Newman black holes, while at $r = 4b/3$ it reads

$$a_{\text{ph-ex}}(r = 4b/3, b) = \pm \frac{\sqrt{b}}{3\sqrt{3}} (8b - 9). \quad (89)$$

The position, value and kind of the extrema of the function $a_{\text{ph}}(r, b)$ are listed in Table (I). The results are summarized in Figure (4). We see that all curves drawn there – the curve $a_{\text{ph-ex}}(r = 4b/3, b)$, the line $a^2 + b = 1$ (corresponding to the extremal black holes), the line $a^2 + b = 0$, and the line $b = 1$ (separating the braneworld Kerr–Newman naked singularities with the ergosphere from those without it) – divide the b - a plane into ten regions. In this sense, the braneworld Kerr–Newman spacetimes can be divided into ten different classes, characterized by:

1. existence of the horizon
2. existence of the ergosphere
3. the number of stable and unstable circular photon orbits.

The situation is summarized in Table (II) and is also visualized in Figure (4), in accord with the analysis of circular photon orbits in the standard Kerr–Newman spacetimes [52]. In the case of the braneworld Kerr–Newman black holes new regions VIII, IX and X corresponding to negative values of the tidal charge, ($b < 0$), occur in addition to the standard Kerr–Newman spacetimes.

V. STABLE CIRCULAR GEODESICS

It is well known that character of the test particle (geodesic) circular motion governs structure of the Keplerian (geometrically thin) accretion disks orbiting a black hole [56, 57] or a naked singularity (superspinar) [36, 37];

Class	Horiz.	Ergo.	Orbits	Class	Horiz.	Ergo.	Orbits
I	yes	yes	0,2	VI	no	yes	2,2
II	yes	yes	1,3	VII	no	no	2,2
III	no	yes	1,1	VIII	yes	yes	0,2
IV	no	no	1,1	IX	yes	yes	0,3
V	no	no	0,0	X	no	yes	0,1

TABLE II. Ten possible divisions of braneworld Kerr–Newman spacetimes with respect to existence of the horizon, existence of the ergosphere and the number of stable and unstable circular photon orbits. The first number in the column orbits corresponds to amount of stable circular photon orbits, the second corresponds to amount of unstable circular photon orbits.

similarly, it can govern also motion of a satellite orbiting the black hole or the naked singularity (superspinar) along a quasicircular orbit slowly descending due to gravitational radiation of the orbiting satellite [60]. The Keplerian accretion, starting at large distances from the attractor, is possible in the regions of the black hole or naked singularity spacetimes where local minima of the effective potential exist and the energy corresponding to these minima decreases with decreasing angular momentum [12]. In other words, in terms of the radial profiles of the quantities characterizing circular geodesics, the Keplerian accretion is possible where both specific angular momentum and the specific energy of circular geodesics decrease with decreasing radius. In the standard model of the black hole accretion disks, the inner edge of the accretion disk is located in the so called marginally stable circular geodesic where the effective potential has an inflexion point [56], but the situation can be more complex in the naked singularity spacetimes [15, 61].

We study stability of the circular geodesic motion of test particles relative to the radial perturbations in the braneworld Kerr–Newman spacetimes. Note that the equatorial circular motion is then always stable relative to the latitudinal perturbations perpendicular to the equatorial plane [62]. We show that the most interesting and, in fact, unexpected result occurs for test particles orbiting the special class of the braneworld mining-unstable Kerr–Newman naked singularities demonstrating an infinitely deep gravitational well enabling (formally) unlimited energy mining from the naked singularity spacetime. Of course, such a mining must be limited by violation of the assumption of the test particle motion.

A. Marginally stable circular geodesics

The loci of the stable circular orbits are given by the condition related to the radial motion $R(r)$ function

$$\frac{\partial^2 R(r, a, b, E, L)}{\partial r^2} \leq 0, \quad (90)$$

or the relation

$$\frac{\partial^2 V_{\text{Eff}}(r, a, b, L)}{\partial r^2} \leq 0, \quad (91)$$

related to the effective potential $V_{\text{Eff}}(r)$, where the case of equality corresponds to the marginally stable circular orbits at r_{ms} with $L = L_{\text{ms}}$, corresponding to the inflexion point of the effective potential – for lower values of the specific angular momentum L the particle cannot follow a circular orbit. Such marginally stable circular orbit represents the innermost stable circular orbit and the inner edge of the Keplerian disks in the Kerr black hole and naked singularity spacetimes.

Using the relations (55) and (56), we obtain for the braneworld Kerr–Newman spacetimes [28][63]

$$r(6r - r^2 - 9b + 3a^2) + 4b(b - a^2) \mp 8a(r - b)^{3/2} = 0. \quad (92)$$

In the previous studies, only the braneworld black hole spacetimes were usually considered [27, 28]. Standard Kerr–Newman naked singularity spacetimes were discussed in [17, 58]. Here we consider whole family of the braneworld Kerr–Newman spacetimes, with both positive and negative tidal charges. The solution of equation (92) can be express in the form

$$a_{\text{ms}} = \mp \frac{4(r - b)^{3/2} \pm \sqrt{3br^2 - (2 + 4b)r^3 + 3r^4}}{4b - 3r}, \quad (93)$$

where the \mp signs correspond to the upper and lower family of the circular geodesics. The \pm signs correspond to the two possible solutions of Eq. (92). The local extrema

of the function $a_{\text{ms}}(r, b)$ are given by the relation

$$a_{\text{ms}(\text{extr})} \equiv \mp \left(2\sqrt{b} \pm \sqrt{b(4b - 1)} \right). \quad (94)$$

Thus it can be shown that there is no solution for equation (92) related to the lower family of circular geodesics when

$$b > \frac{5}{4} \quad \wedge \quad a < -2\sqrt{b} + \sqrt{b(4b - 1)} \quad (95)$$

and there is no solution for the upper sign family of circular geodesics when $1 > b > 1/4$ and

$$2\sqrt{b} - \sqrt{b(4b - 1)} < a < 2\sqrt{b} + \sqrt{b(4b - 1)}. \quad (96)$$

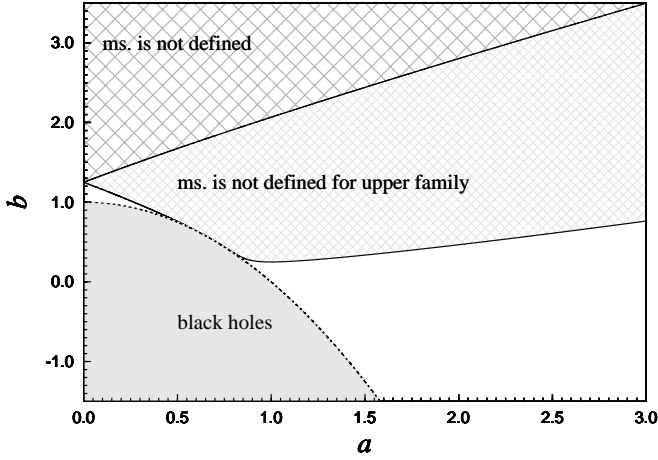


FIG. 5. Mapping of existence of the marginally stable circular geodesics in the parameter space of the braneworld Kerr–Newman spacetimes.

The existence of the marginally stable circular geodesics in dependence on the dimensionless parameters of the braneworld Kerr–Newman spacetimes is represented in Figure (5). This figure will be crucial for construction of the classification of the Kerr–Newman spacetimes according to the Keplerian accretion, but it is not sufficient, as the classification of the photon circular geodesics plays a crucial role too.

The function $a_{\text{ms}}(r, b)$ determines in a given Kerr–Newman spacetime location of the marginally stable circular geodesics that are usually considered as the boundary of Keplerian accretion discs determined by the quasi-geodesic motion.

B. Innermost stable circular geodesics

The standard treatment when the inner edge of the Keplerian accretion discs is located at the marginally stable orbits defined by the inflexion point of the effective potential (this point is also the innermost stable circular orbit (ISCO) [56]) works perfectly in the braneworld Kerr–Newman black hole spacetimes, but the situation is more complex in the braneworld naked singularity spacetimes, as the innermost stable circular orbits (ISCO) do not always correspond to the marginally stable orbit defined by equation (92)[64]. The ISCOs that are not coinciding with a marginally stable circular geodesic, related to an inflexion point of the effective potential, correspond to the orbits with lowest radius in sequence of stable circular geodesics. Contrary to the case of the marginally stable circular orbits from which the particles can move inwards, in the case of ISCO representing the inner limit of stable circular geodesics the particle remains captured at this orbit or in its vicinity. Such ISCO orbits were found for the first time in the Reissner–Nordström(-de Sitter) naked singularity spacetimes when they correspond to

orbits with vanishing angular momentum (particles at static positions) [15, 16]. Here we demonstrate existence of a new class of this kind of ISCO representing the limit of stable circular geodesics located at the stable photon circular geodesic. In order to allow for the standard accretion with decreasing E and L with decreasing radius of the stable orbits, we have considered the stable circular geodesics with $E \rightarrow -\infty$ and $L \rightarrow -\infty$.

The ISCO can be formally determined, if we consider the function of the radius of the circular geodesic $r_c(L_c; a, b)$, given implicitly by Eq.(56), or $r_c(E_c; a, b)$, given implicitly by Eq.(55). Then the r_{ISCO} can be defined in a given spacetime, with fixed parameters a, b , by the relations $dr_c/dL_c = 0$, $dr_c/dE_c = 0$ that can be expressed as $dL_c/dr_c \rightarrow -\infty$ and $dE_c/dr_c \rightarrow -\infty$, related to the standard accretion with decreasing energy and angular momentum of accreting matter. Note that the conditions $dL_c/dr_c \rightarrow \infty$ and $dE_c/dr_c \rightarrow \infty$ can determine the outermost stable circular geodesics from which the accretion could start, but such a situation is not related to plausible astrophysical situation as discussed in detail in [61].

There are two relevant cases when the conditions $dL_c/dr_c \rightarrow \pm\infty$ and $dE_c/dr_c \rightarrow \pm\infty$ can be satisfied:

$$\text{a) } 0 = r^2 - 3r + 2b \pm 2a\sqrt{r-b}, \quad (97)$$

$$\text{b) } r = b. \quad (98)$$

The case a) tells us that the innermost circular geodesics corresponds to the photon circular geodesics that can be also stable with respect to radial perturbations so that this condition is also applicable as a limit on the stable circular orbits of test particles, as demonstrated in [15]. Then the specific energy and the specific angular momentum tend asymptotically to $E \rightarrow \pm\infty$ and $L \rightarrow \pm\infty$ but the impact parameter $\lambda = L/E$ remains finite. The condition $r > b$ could restrict the condition implied by the photon circular geodesics. Here we consider the case of $dL_c/dr_c \rightarrow -\infty$ and $dE_c/dr_c \rightarrow -\infty$.

The case b) can be relevant for the braneworld spacetimes with positive braneworld parameter b , as demonstrated in [15] where the effective potential $V_{\text{eff}}(r, b, L)$ for the Reissner–Nordström naked singularity spacetimes clearly demonstrates that the inner edge of the Keplerian disc is located at $r = b$, having $L = 0$, while no marginally stable circular orbit, corresponding to an inflexion point of the effective potential, exist. Note that in some spacetimes the sequence of the stable circular geodesics can start at the outermost stable circular geodesic with $dL_c/dr_c \rightarrow +\infty$ and $dE_c/dr_c \rightarrow +\infty$ corresponding to the stable circular geodesic.

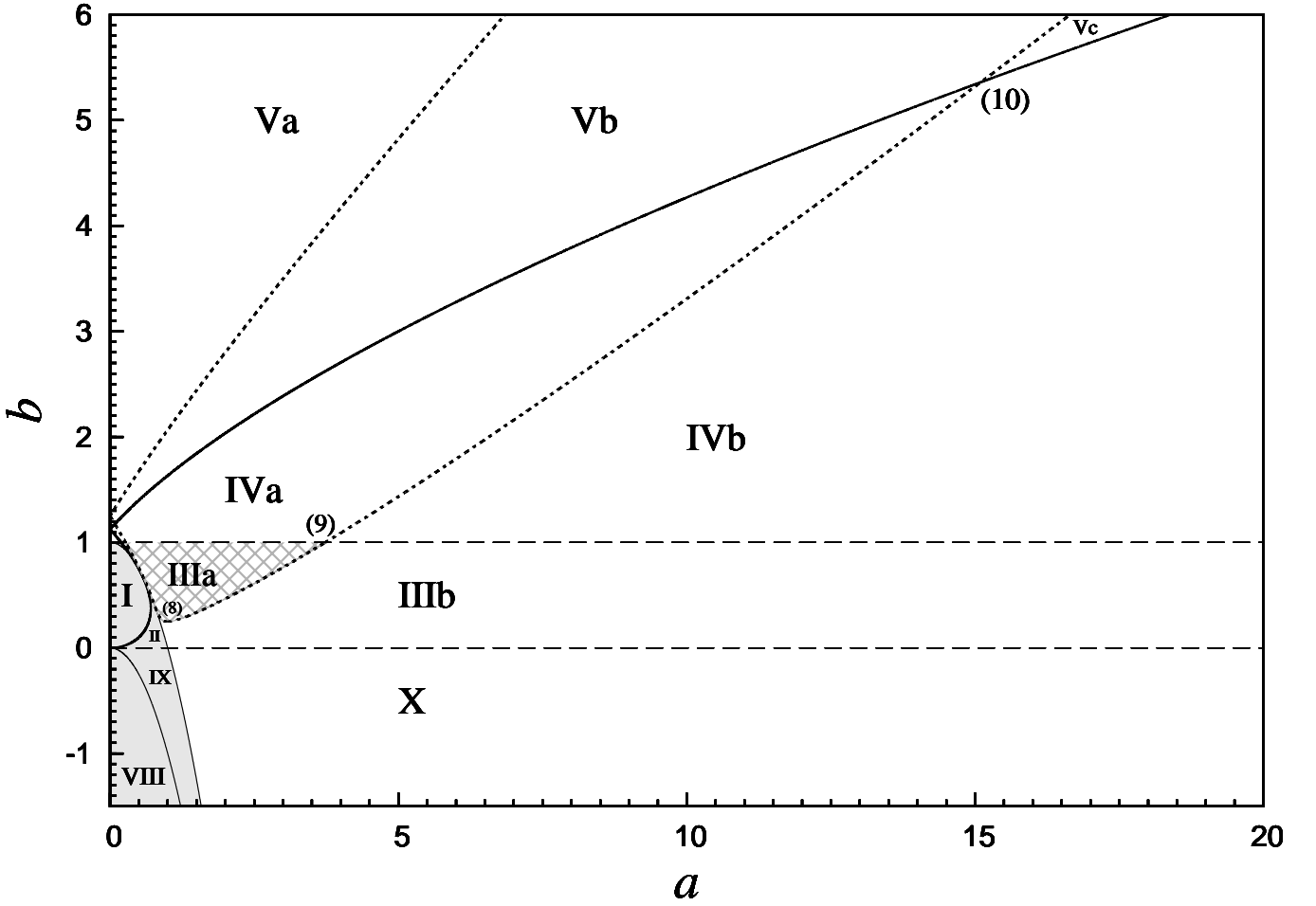


FIG. 6. Classification of the braneworld Kerr–Newman spacetimes according to the properties of circular geodesics relevant for the Keplerian accretion. The parameter space $b - a$ is separated by curves governing the extrema of the functions determining the photon circular orbits (thick lines) and the marginally stable orbits (dashed lines). Point $(\sqrt{0.5}, 0.5)$ is an intersection of dashed line and curve separating black holes from naked singularities ($b = 1 - a^2$). This two curves are tangent at the common point.

C. Effective potential dependence on specific angular momentum and analytical proof that Keplerian accretion with infinite efficiency can exist in approximation of geodesic motion

The Keplerian accretion works if there exist a continuous sequence of local minima of the effective potential with decreasing values of angular momentum L . In terms of the effective potential (67), the conditions for existence of Keplerian accretion disks can be express in the form

$$\begin{aligned} \frac{\partial V_{\text{Eff}}(r, a, b, L)}{\partial r} &= 0, \\ \frac{\partial^2 V_{\text{Eff}}(r, a, b, L)}{\partial r^2} &\leq 0, \\ \frac{\partial V_{\text{Eff}}(r, a, b, L)}{\partial L} &< 0. \end{aligned} \quad (99)$$

Except the possibility to stop this procedure by the inflexion point of the effective potential, there exist other

possible way to stop validity of these conditions:

$$\frac{\partial V_{\text{Eff}}(r, a, b, L)}{\partial L} = 0 \quad (100)$$

that will be satisfied at a turning point where

$$L = L_T \equiv \frac{\pm a(2r - b)}{r\sqrt{r^2 - 2r + b}}. \quad (101)$$

At this turning point the minimum of effective potential, given by $\partial V_{\text{Eff}}(r, a, b, L_T)/\partial r = 0$, is located where:

$$\frac{r - b}{r^2\sqrt{r^2 - 2r + b}} = 0 \Rightarrow r = b. \quad (102)$$

In such situations, the inner edge of the Keplerian accretion disk is located at $r = b$. Putting this result into the definition of the function L_T , we find

$$L_T(r = b) = \frac{\pm ab}{b\sqrt{b(b-1)}} \Rightarrow b > 1. \quad (103)$$

We see that the effect of existence of the lowest possible value of angular momentum L associated with local minima of effective potential occurs only for values of the tidal charge $b > 1$ when equation (102) is well defined at $r > b$.

The second possible way the conditions (99) are not well matched is related to the situation when the local minima of the effective potential turn into an inflexion point at r defined by (92).

So the inflexion point of the effective potential is not always defined, if the tidal parameter $b > 5/4$ for the lower family solution of equation (92). In this case the Keplerian accretion stops at the point $r = b$ where the minimum of the effective potential starts to increase in energy level with decreasing L .

On the other hand, for the upper family solution of equation (92) situation becomes extraordinary and much more interesting for the tidal charge in the interval $1 > b > 1/4$, and appropriately tuned spin a ; then the inflexion point of the effective potential does not exist – for this reason, the Keplerian accretion starting at large values of the angular momentum of accreting matter cannot be stopped, and it continues with no limit to unlimitedly large negative values of the angular momentum and unlimitedly large negative values of the energy.

Therefore, in this case, unrestricted mining of the energy due to the Keplerian accretion could occur. Of course, this mining has to be stopped at least when the energy of the accreting matter starts to be comparable to the mass parameter of the Kerr–Newman naked singularity, and the approximation of the test particle motion of matter in the disk is no longer valid.

VI. CLASSIFICATION OF BRANEWORLD KERR–NEWMAN SPACETIMES ACCORDING TO RADIAL PROFILES OF CIRCULAR GEODESICS

In order to create classification of the braneworld Kerr–Newman black hole and naked singularity spacetimes according to possible regimes of the Keplerian accretion, we consider existence of the event horizons, existence of the ergosphere, and we use the characteristics of the circular geodesics: existence of the circular photon geodesics and their stability, existence of the marginally stable circular geodesics related to inflexion points of the effective potential, and relevance of the limiting radius $r = b$. We use the classification of the braneworld Kerr–Newman spacetimes introduced for the characterization of the photon circular geodesics, and generate a subdivision of the introduced classes according to the criteria related to the marginally stable orbits.

The individual classes of the Kerr–Newman spacetimes will be represented by typical radial profiles of the specific angular momentum L , specific energy E , and the effective potential V_{eff} that enable understanding of the Keplerian accretion and calculation of its efficiency. We

first briefly summarize results of the two special cases – Kerr and Reissner–Nordström spacetimes. In the following classification of the braneworld Kerr–Newman spacetimes the characteristic types of the behaviour of the circular geodesics in the special Kerr and Reissner–Nordström spacetimes occur, but also some quite new and extraordinary situations arise. The results of the circular geodesic analysis in the braneworld Kerr–Newman spacetimes can be directly applied also for the circular geodesics in the standard Kerr–Newman spacetimes, if we make transformation $b \rightarrow Q^2$ where Q^2 represents the squared electric charge parameter of the Kerr–Newman background.

A. Case $b=0$: Kerr black hole and naked singularity spacetimes

The limiting case of the well known results of the test particle circular orbits in the Kerr spacetimes that were studied in detail in [35, 43] demonstrates clearly the necessity of very careful treating of the families of circular orbits in the naked singularity spacetimes where the simple decomposition of the circular orbits to corotating and counterrotating (retrograde) is not always possible. Namely, in the spacetimes with $1 < a < a_c = 1.3$ the circular orbits that are corotating at large distances from the ring singularity become retrograde near the ring singularity, at the ergosphere; moreover, in the spacetimes with $1 < a < a_0 = 1.089$ the covariant energy of such orbits can be negative. The specific energy and specific angular momentum of the circular geodesics of the Kerr black hole and naked singularity spacetimes are illustrated in Figure (8). Notice that the unstable circular geodesics approach the radius $r = 0$ with unlimitedly increasing covariant energy and axial angular momentum, however, the photon circular geodesic cannot exist at the ring singularity. The Kerr naked singularities are classically unstable as Keplerian accretion from both the corotating and counterrotating disks inverts the naked singularity into an extreme Kerr black hole – the transition is discontinuous (continuous) for corotating (counterrotating) Keplerian disk [34–36, 65]. We shall see later that the Keplerian accretion cannot be generally treated simply in the Kerr–Newman naked singularity spacetimes due to the complexities discussed in detail in [61]. We expect addressing this issue in future work.

B. Case $a=0$: Reissner–Nordström black hole and naked singularity spacetimes

The other limiting case of the Reissner–Nordström (RN) and Reissner–Nordström-(anti-)de Sitter black hole and naked singularity spacetimes has been treated in [15, 16]. It has been demonstrated that in the Reissner–Nordström naked singularity spacetimes even two sepa-

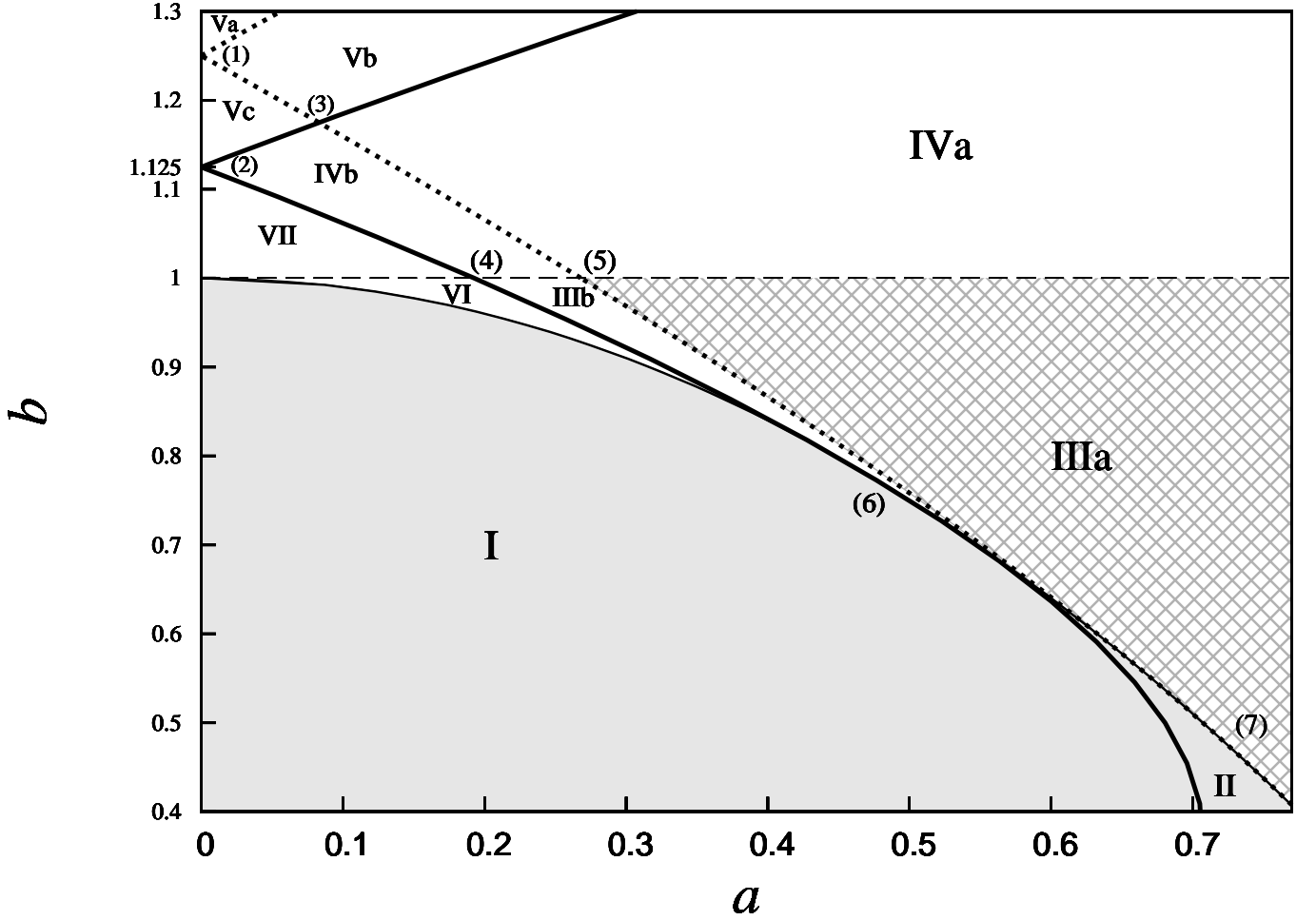


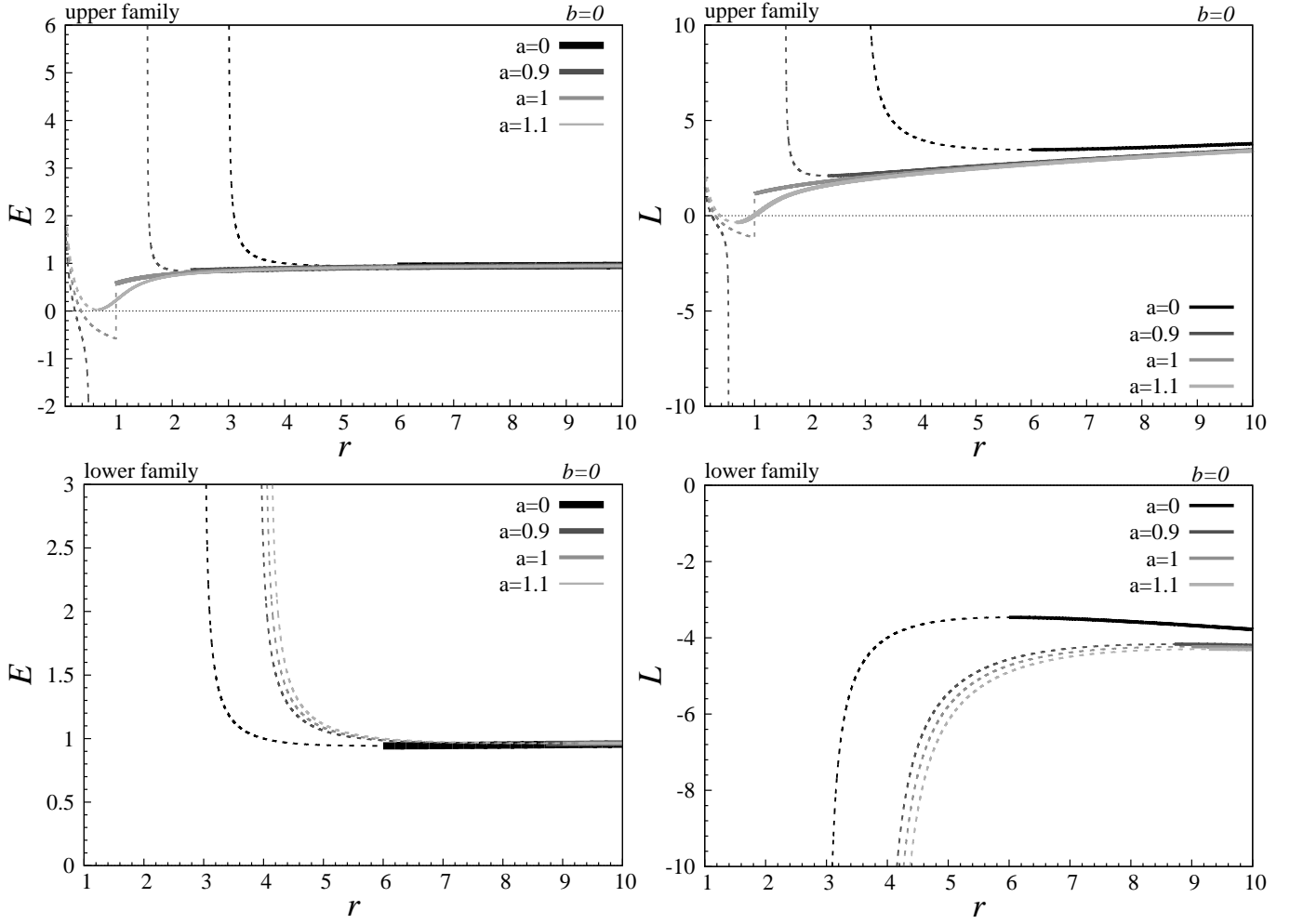
FIG. 7. Classification of the braneworld Kerr–Newman spacetimes according to the properties of circular geodesics relevant for the Keplerian accretion. The parameter space $b - a$ is separated by curves governing the extrema of the functions determining the photon circular orbits (thick lines) and the marginally stable orbits (dashed lines). Detailed structure for small values of spin a and $b \sim 1$.

rated regions of circular geodesics could exist. The doubled regions of the stable circular motion occur in the RN naked singularity spacetimes with the charge parameter $1 < Q^2 < 5/4$, or even only stable circular geodesics could exist, if the charge parameter $Q^2 > 5/4$. In the RN naked singularity spacetimes also doubled photon circular geodesics can occur, with the inner one being stable relative to radial perturbations, if the charge parameter is in the interval of $1 < Q^2 < 9/8$ [15, 17]. The same phenomena occur in the naked singularity Kehagias–Sfetsos spacetimes of the Hořava quantum gravity [61, 66] or in the no-horizon regular Bardeen or Ayon–Beato–Garcia spacetimes [67, 68].

We shall see that in the braneworld Kerr–Newman naked singularity spacetimes the special naked singularity effects of the Kerr and Reissner–Nordström case are mixed in an extraordinary way leading to existence of an infinitely deep gravitational well implying the new effect we call mining instability.

C. Characteristic points of the Kerr–Newman spacetime classification

The classification of the braneworld Kerr–Newman spacetimes according to the character of the circular geodesics and related effective potential are determined by the functions governing the local extrema of the functions giving the photon circular geodesics and the marginally stable circular geodesics corresponding to the inflexion points of the effective potential. In the space of the spacetime parameters $b - a$ then exist fourteen regions corresponding to classes of the braneworld Kerr–Newman spacetimes demonstrating different behaviour of the circular geodesics and Keplerian accretion as demonstrated in Figure (6) and in Figure (7) giving details of the regions of low values of the dimensionless parameters a and b . These regions are governed by intersection points of the curves (88) and (94) that give thirteen characteristic points in the parameter space that

FIG. 8. E and L for Kerr black hole and naked singularities.

are summarized in the following way: the pairs (a, b) are ordered gradually from the top to the bottom and from

the left to the right,

- (1) $\rightarrow (0, 1.25)$,
- (2) $\rightarrow (0, 1.125)$,
- (3) $\rightarrow \left(\frac{A_- (12 + A_-)}{16\sqrt{2}}, \frac{3}{32} (12 + A_-) \right) = (0.0831, 1.1748)$,
- (4) $\rightarrow \left(\frac{1}{3\sqrt{3}}, 1 \right) = (0.19245, 1)$,
- (5) $\rightarrow (2 - \sqrt{3}, 1) = (0.268, 1)$,
- (6) $\rightarrow \left(0.5, \frac{3}{4} \right)$,
- (7) $\rightarrow (\sqrt{0.5}, 0.5)$,
- (8) $\rightarrow (1, 0.25)$,
- (9) $\rightarrow (2 + \sqrt{3}, 1) = (3.732, 1)$,
- (10) $\rightarrow \left(\frac{A_+ (12 + A_+)}{16\sqrt{2}}, \frac{3}{32} (12 + A_+) \right) = (15.0992, 5.361)$,

Class	ISCO	MSO(u)	MSO(l)	Hor./Erg.	SP	UP
I	=MSO	classic	classic	yes/yes	0	2
II	=MSO	classic	classic	yes/yes	1	3
IIIa	=Photon	—	classic	no/yes	1	1
IIIb	=MSO	classic	classic	no/yes	1	1
IVa	at $r=b$	—	classic	no/no	1	1
IVb	at $r=b$	classic	classic	no/no	1	1
Va	at $r=b$	—	—	no/no	0	0
Vb	at $r=b$	—	classic	no/no	0	0
Vc	at $r=b$	classic	classic	no/no	0	0
VI	=MSO	classic	classic	no/yes	2	2
VII	at $r=b$	classic	classic	no/no	2	2
VIII	=MSO	classic	classic	yes/yes	0	2
IX	=MSO	classic	classic	yes/yes	0	3
X	=MSO	classic	classic	no/yes	0	1

TABLE III. Classification of parameter space $b - a$ with respect to: ISCO - radius of innermost stable circular orbit; MSO(u) - radius of Marginally Stable Orbit for upper sign family; MSO(l) - radius of Marginally Stable Orbit for lower sign family; SP - number of stable photon circular orbit; UP - number of unstable photon circular orbit. ISCO has only two possible outcomes. It can be identical with MSO or lies at $r = b$. Word “classic” in this context means that MSO is defined by equation (92).

where

$$A_{\pm} = \left(9 + 8\sqrt{3} \pm \sqrt{3(83 + 48\sqrt{3})} \right) \quad (104)$$

The point (6) is the crossing point of the function of the extrema of the photon circular orbit function $a_{\text{ph-ex}}$, and the curve separating black hole and naked singularity spacetimes, $b = 1 - a^2$. The point (7) is the common point of the dotted curve, given by the function $a_{\text{ms(extr)}}$ and limiting the spacetimes allowing for existence of the marginally stable orbits, and the curve separating black holes from naked singularities ($b = 1 - a^2$). These two curves are tangent at the common point.

D. Character of circular geodesics in the Kerr–Newman spacetimes

The parameter space of the braneworld Kerr–Newman spacetimes $b - a$ is divided into fourteen regions due to the criteria reflecting basic properties of the spacetimes and properties of their circular geodesics:

- Existence of event horizons and ergosphere
- Existence of unstable and stable circular photon geodesics
- Existence of the marginally stable geodesics or the innermost stable circular geodesics (ISCO)

The classification is summarized in Table (III). Basically, we combine Figure (5) with Figure (4) to obtain Figures (6,7) where properties of the photon circular geodesics and properties of marginally stable geodesics or ISCO’s are reflected. We will show that the most surprising properties of the Keplerian accretion arise in the spacetimes of Class IIIa.

Now we give properties of the circular geodesics in all the fourteen classes of the braneworld Kerr–Newman spacetimes, presenting and discussing typical radial profiles of their specific energy and specific angular momentum, complemented by sequences of the effective potential. Classification of the standard Kerr–Newman spacetimes according to properties of the circular geodesics contains all the classes except those related to $b < 0$ – therefore, classes VIII, IX and X are excluded.

1. Class I

Class of the black hole spacetimes with two horizons, two unstable photon circular orbits and ergosphere. Class border is given by line $b = a_{\text{ph-ex}}(r = 4b/3, b)$, $b = 1 - a^2$ with intersection at point (0.5, 3/4) (point number (6) in Figure (6)) and line $a = 0$.

Marginally stable orbits for test massive particles are given by the inflexion point of the effective potential are defined by equation (92) and coincide with the ISCO’s (this is the standard scenario of Keplerian accretion: shortly – classic).

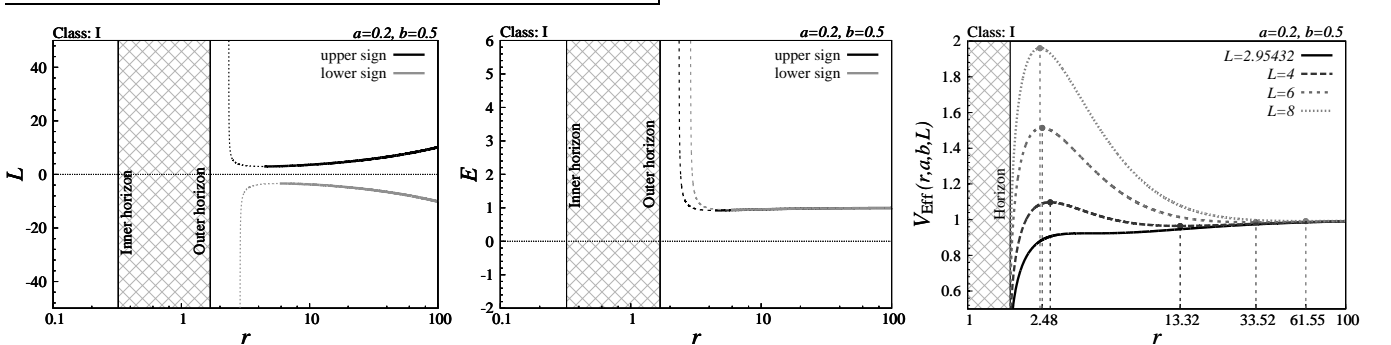


FIG. 9. L , E and effective potential for class I.

2. Class II

Class of the black hole spacetimes with two horizons, one stable and three unstable photon circular orbits and ergosphere. Notice that the stable and unstable photon circular geodesic are located under the inner horizon, being thus irrelevant for the Keplerian accretion. Border is

given by line $b = a_{\text{ph-ex}}(r = 4b/3, b)$ and $b = 1 - a^2$ with intersection at point (0.5, 3/4) (point number (6) in figure (6)) and line $b = 0$.

Marginally stable orbits for test massive particles are given by the inflexion point of the effective potential, coinciding with the ISCO's (classic).

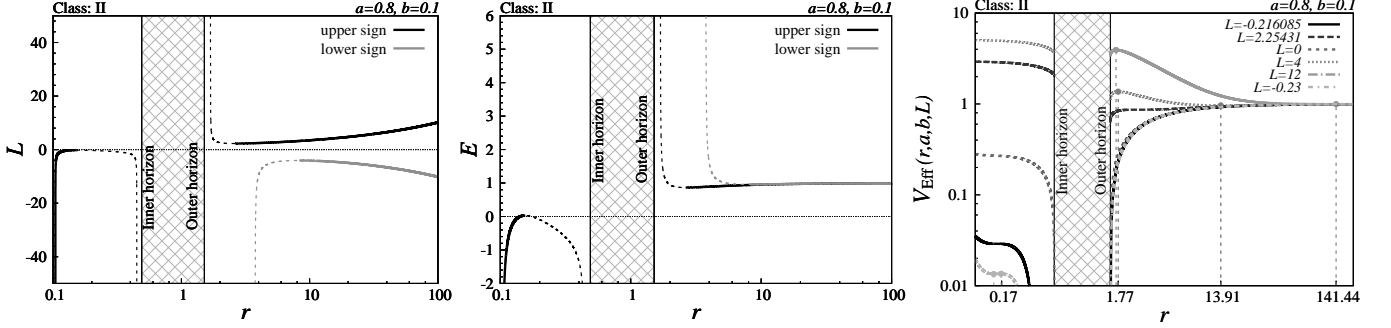


FIG. 10. L , E and effective potential for class II.

3. Class IIIa

Class of the naked singularity spacetimes with one stable and one unstable photon circular geodesics and ergosphere. The border of the Class IIIa region is given by line $b = a_{\text{ms(extr)}}$ and line $b = 1$ with intersection points at $(2 - \sqrt{3}, 1) = (0.268, 1)$ (point number (5)) and $(2 + \sqrt{3}, 1) = (3.732, 1)$ (point number (9)). We have also marked the point number (7) with coordinates $(\sqrt{0.5}, 0.5)$ where the line $b = a_{\text{ms(extr)}}$ and line $b = 1 - a^2$ touch

and are tangent to each other. This theoretically means that effect of mining instability can be achieved for extremal Kerr–Newman black holes with spin parameter $a = \sqrt{0.5}$ and charge or braneworld tidal charge parameter $b = 0.5$. But it occurs under the event horizon. We have also marked the point number (8) with coordinates (1, 0.25) giving information on minimal amount of electric charge or braneworld tidal charge parameter b .

Marginally stable orbit of massive test particles is in case of the lower family circular geodesics given by inflexion point of the effective potential and coincides with the ISCO (classic).

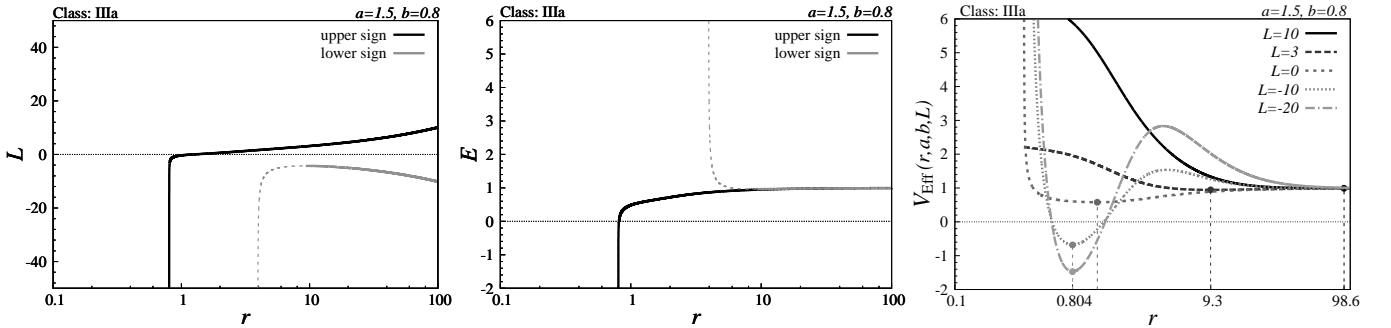


FIG. 11. L , E and effective potential for class IIIa.

In case of the upper family circular geodesics, the inflexion point of the effective potential is not defined and the sequence of minima of the effective potential continues with decreasing specific energy and specific angular

momentum of the accreting matter down to the stable photon orbit. This orbit can be therefore considered as ISCO of the massive test particles. We have thus found an infinitely deep gravitational well enabling theoretically

an unlimited mining of energy from the naked singularity. In fact, such a mining instability could work only up to the energy contained in the naked singularity spacetime. We can expect that the energy mining could work also in more realistic situations when the naked singularity is removed and an astrophysically more plausible superspinar is created by joining a regular (e.g. stringy) solution to the Kerr–Newman spacetime at a radius overcoming the outer radius of the causality violation region [37, 40]. The mining could work if the matching radius of the internal stringy spacetime and the outer

Kerr–Newman spacetime is smaller than the radius of the stable photon orbit related to the mining instability of the Class IIIa spacetimes.

For completeness, we give in this case also the locally measured (LNRF) specific energy of the upper family circular geodesics. As shown in Figure 12, the specific energy E_{LNRF} diverges, along with the covariant specific energy E as the orbit approaches the limiting photon circular orbit. On the other hand, Figure 13 clearly demonstrates that the ratio $|E|/E_{LNRF}$ remains finite while the orbits approach the location corresponding to the stable photon circular orbit.

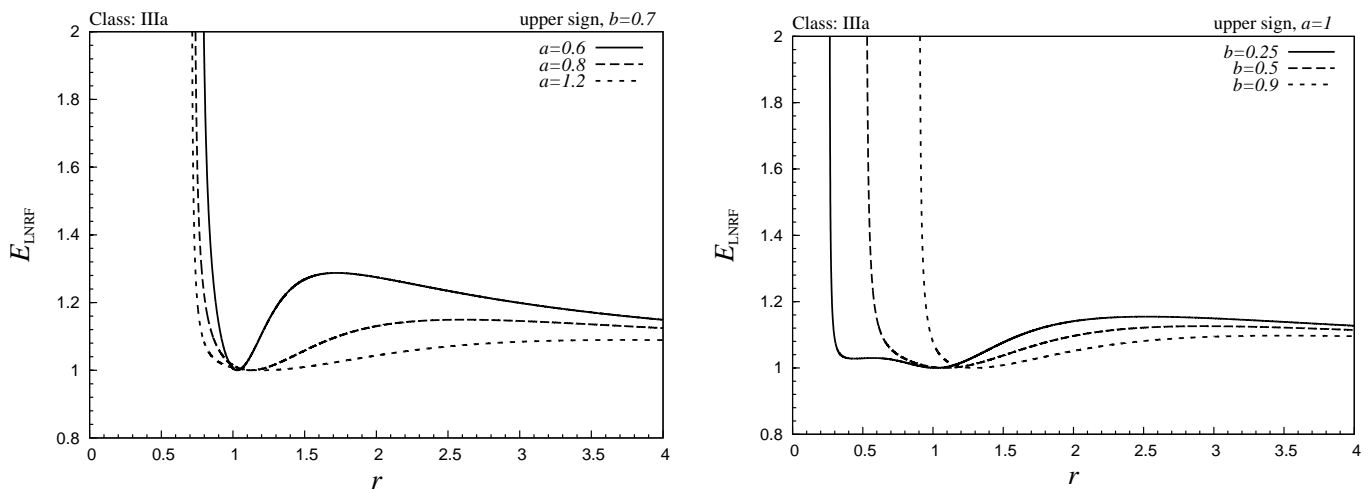


FIG. 12. Energy measured by the LNRF observers (upper sign family orbits only) in the mining unstable Kerr–Newman spacetimes of class IIIa. The energy diverges at the radius of the stable photon circular orbit.

Of course, the mining instability could work only if the assumption of the test particle motion of the accreting matter is satisfied. Therefore, the assumption requires validity of the relation

$$|\tilde{E}| \ll M, \quad (105)$$

the covariant energy of the particle (accreting matter)

has to be much smaller than the naked singularity mass parameter M . Of course, the issue of the mining instability and the related interaction of the mining unstable Kerr–Newman naked singularity (Kerr–Newman superspinar) and the accreting mass is much more complex and deserves a more detailed study.

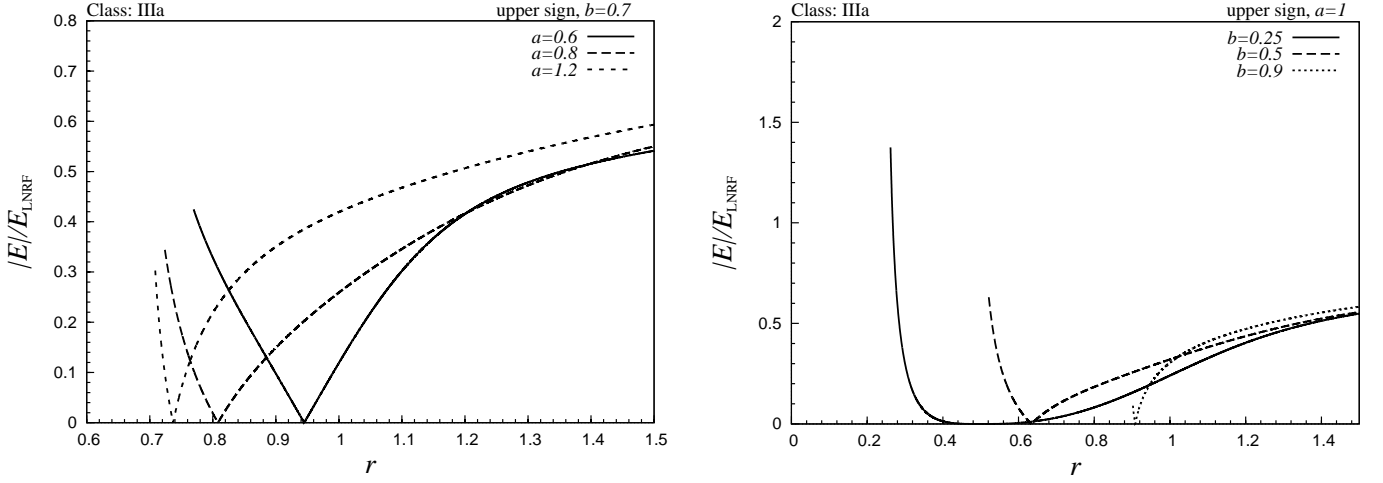


FIG. 13. Absolute value of covariant energy $|E|$ divided by LNR energy (for the upper sign family orbits) in the mining unstable Kerr-Newman spacetimes of class IIIa. The fraction is defined down to the radius of the stable circular photon orbit and at this point it has a finite value.

4. Class IIIb

Class of naked singularity spacetimes with one stable and one unstable photon circular orbit and ergosphere. In the parameter space $b-a$ the area related to this class is not compact and disintegrates into two separated areas. The first area is infinitely large, its border is given by the line $b = a_{\text{ms(extr)}}$, line $b = 1 - a^2$, line $b = 1$ and $b = 0$ with intersections at the point $(\sqrt{0.5}, 0.5)$ (point number (7)) and $(2 + \sqrt{3}, 1)$ (point number (9)). The second area is compact and finite. Its border is given by the line $b = a_{\text{ms(extr)}}$, line $b = a_{\text{ph-ex}}(r = 4b/3, b)$, line $b = 1 - a^2$ and line $b = 1$ with intersection points number (4), (5) and (7). It is not obvious from figures, but $b = a_{\text{ms(extr)}}$ and $b = a_{\text{ph-ex}}(r = 4b/3, b)$ do not

intersect.

Marginally stable orbits of both the lower and upper family of circular geodesics are given by the inflexion point of the effective potential and coincide with ISCO's (classic). Notice that in this case the sequence of the upper family orbits with descending specific energy E and specific angular momentum L is interrupted by a sequence where both E and L increase with decreasing radius, corresponding thus to the unstable geodesics. In this case, the infinitely deep gravitational well still exists, but the Keplerian accretion sequence is interrupted and this gravitational well cannot be applied in an astrophysically natural accretion process. Nevertheless, it is still possible to use this gravitational well, if matter with appropriate initial conditions (values of the motion constants), enabling starting of the mining instability, could appear close to the naked singularity.

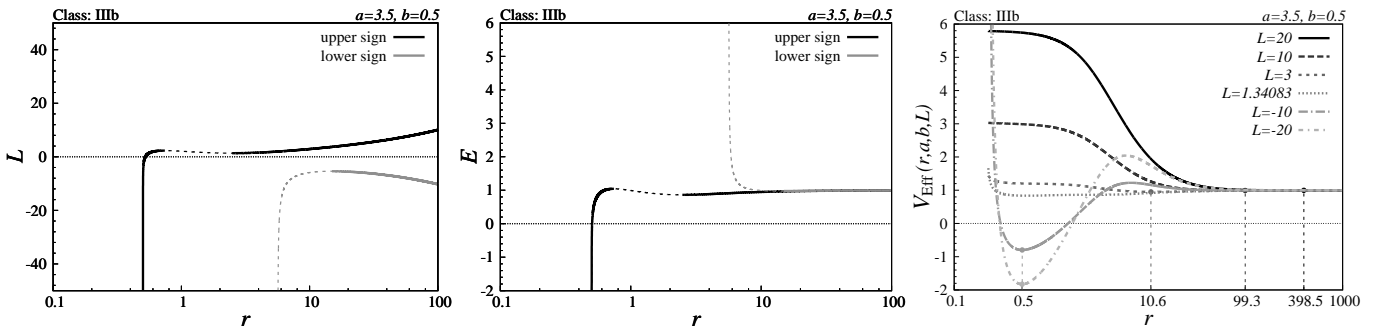


FIG. 14. L , E and effective potential for class IIIb.

5. Class IVa

Class of naked singularity spacetimes with one stable and one unstable photon circular orbit. Class is without

ergosphere. Border of this class in the spacetime parameter space is given by line $b = a_{\text{ph-ex}}(r = 4b/3, b)$ and

$b = a_{\text{ms}(\text{extr})}$ with intersection points (3),(5),(9) and (10).

For the lower family circular geodesics, the marginally stable orbits defined by the inflexion point of the effective potential occur (classic). For the upper family circular geodesics marginally stable orbit is not defined, and the ISCO is located at $r = b$ as it is always for all classes with $b > 1$. A sequence of stable circular geodesics with

sharply increasing specific energy occurs near (above) the radius $r = b$, approaching the stable photon circular orbit. (Such sequences of stable circular orbits were discussed in [61].)

Note that probability we are actually living in a space-time with the braneworld tidal charge parameter greater than one is very small [26, 27].

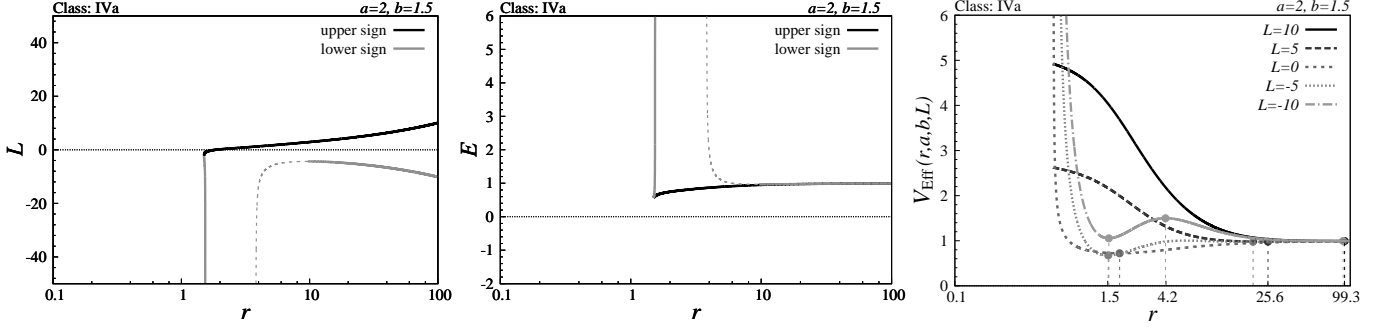


FIG. 15. L , E and effective potential for class IVa.

6. Class IVb

Class of naked singularity spacetimes with one stable and one unstable photon circular orbit. These spacetimes are without ergosphere. In the parameter space $b - a$, this class is not compact and disintegrates into two separated areas. The first area is infinitely large, the border is given by the line $b = a_{\text{ph}}(4b/3, b)$, line $b = a_{\text{ms}(\text{extr})}$ and line $b = 1$ with intersection points (9) and (10). The second area is finite and its border is given by same lines and

intersection points (2), (3), (4) and (5).

For both the upper and lower families of circular geodesics, the marginally stable orbits of test massive particles are given by the inflexion point of the effective potential, governing the sequence of geodesics related to the standard Keplerian accretion (classic). There is additional internal sequence of stable circular geodesic, with the ISCO located at $r = b$, as it is always for all classes with $b > 1$. This sequence approaches the stable photon circular geodesic at the outer edge.

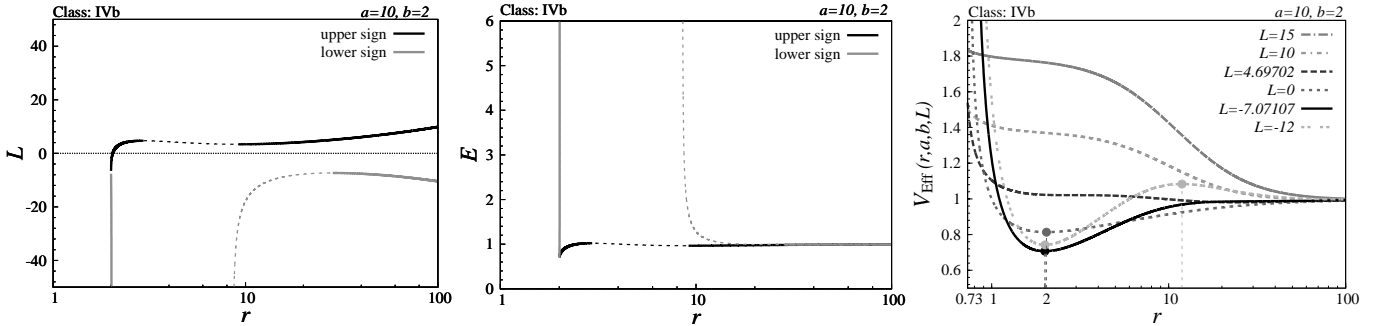


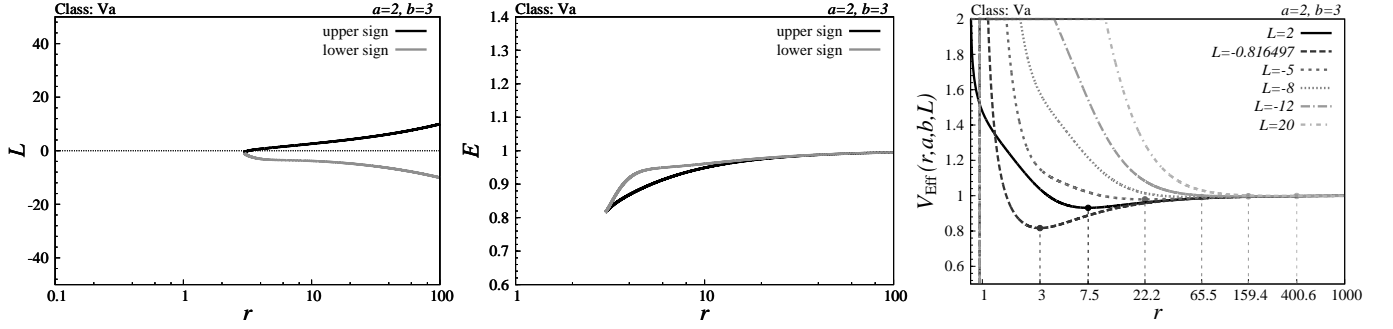
FIG. 16. L , E and effective potential for class IVb.

7. Class Va

Class of naked singularity spacetimes with no stable or unstable photon circular orbit. These spacetimes are also without ergosphere. The border of the Class Va region in the parameter space is given by the line $b = a_{\text{ms}(\text{extr})}$ and

line $a = 0$, with intersection point (1).

For both the lower and upper family circular geodesics, the marginally stable orbits are not defined. The circular geodesics are only stable, the ISCO's are located at $r = b$, as for all the spacetime classes with $b > 1$.

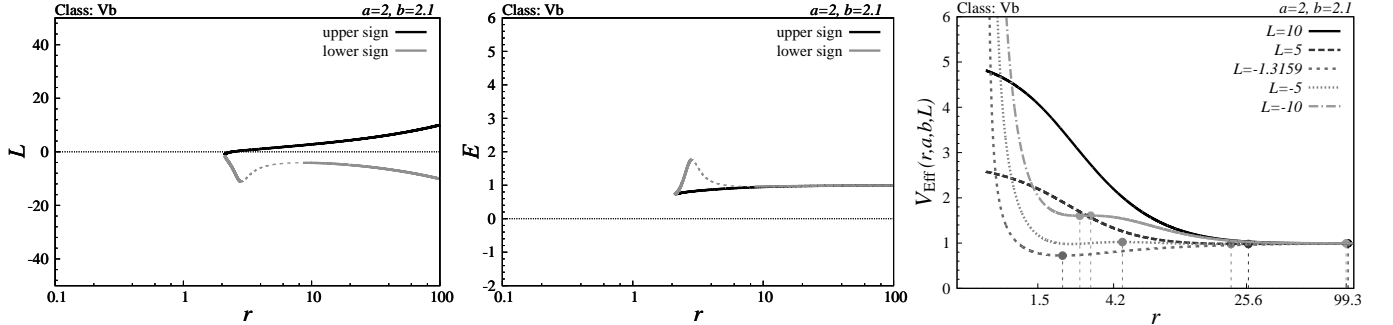
FIG. 17. L , E and effective potential for class Va.

8. Class Vb

Class of naked singularity spacetime with no stable or unstable photon circular orbit. These spacetimes are also without ergosphere. The border of the Class Vb region in the parameter space is given by the line $b = a_{\text{ms}(\text{extr})}$, and line $b = a_{\text{ph}}(4b/3, b)$, with intersection points (1), (3)

and (10). The class is infinitely extended in the parameter space.

The upper family circular geodesics are stable only, finishing at the ISCO located at $r = b$. The marginally stable orbit exists for the lower family orbits, giving the limit of the standard Keplerian accretion. The lower family orbits continue downwards by sequence of unstable orbits and finally stable orbits finishing at $r = b$.

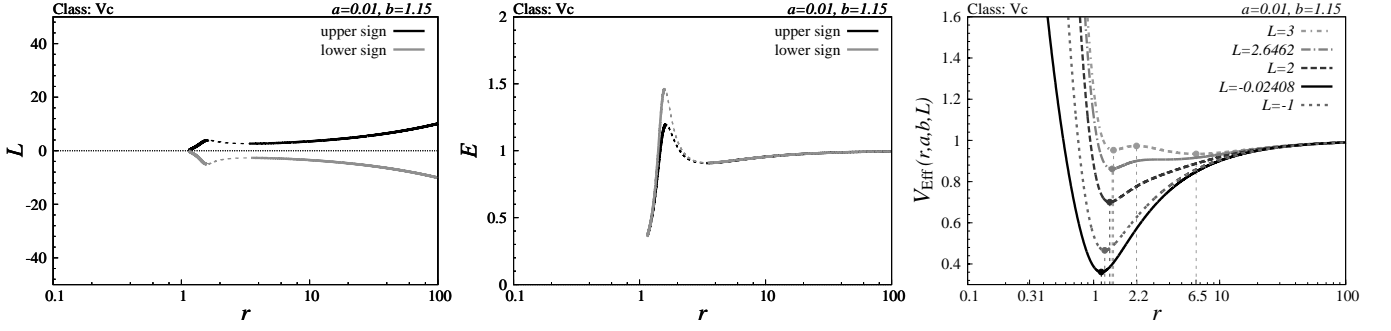
FIG. 18. L , E and effective potential for class Vb.

9. Class Vc

Class of naked singularity spacetimes with no stable or unstable photon circular orbit. These are again spacetimes without ergosphere. In the parameter space $b - a$ this class disintegrates into two separated areas. The first one is infinitely extended, its border is given by the line $b = a_{\text{ph-ex}}(r = 4b/3, b)$ and line $b = a_{\text{ms}(\text{extr})}$, with the intersection point (10). The second area is finite and its

border is given by same line $b = a_{\text{ph-ex}}(r = 4b/3, b)$, line $b = a_{\text{ms}(\text{extr})}$ and line $a = 0$, with intersection points (1), (2) and (3).

The marginally stable orbit exists for both the lower and upper family circular geodesics, giving thus the standard limit of the Keplerian accretion (classic). Both the lower and upper family orbits continue downwards by sequence of unstable orbits and finally stable orbits finishing at $r = b$.

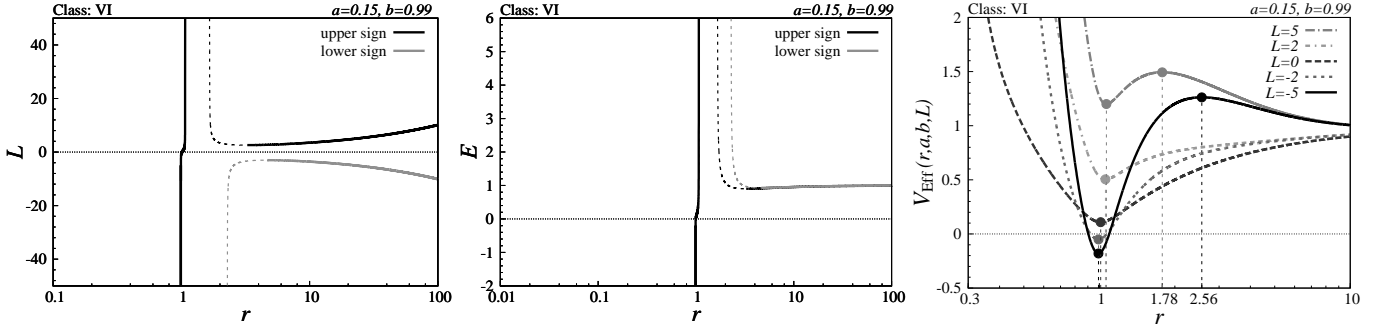
FIG. 19. L , E and effective potential for class Vc.

10. Class VI

Class of naked singularity spacetimes with two stable and two unstable photon circular orbits and ergosphere. In the parameter space the area of the Class VI spacetimes has the boundary given by the line $b = a_{\text{ph-ex}}(r = 4b/3, b)$, line $b = 1 - a^2$ and the line $b = 1$, with the in-

tersection points (4) and (6).

For both the lower and upper family of circular geodesics the marginally stable orbit exists, giving thus the inner edge of the standard Keplerian accretion. The upper family orbits have also a very narrow region of stable circular orbits near the radius $r = b$, starting at the stable circular photon orbit.

FIG. 20. L , E and effective potential for class VI.

11. Class VII

Class of naked singularity spacetimes with two stable and two unstable photon circular orbits, having no ergosphere. In the parameter space the area of the Class VII spacetimes has the boundary given by the line $b = a_{\text{ph-ex}}(r = 4b/3, b)$, line $a = 0$ and the line $b = 1$, with

the intersection points (2) and (4).

For both the lower and upper family circular geodesics, the marginally stable orbit exists giving thus the edge of the standard Keplerian accretion. Further, both the lower and upper family orbits have the ISCO at $r = b$ where sequence of stable orbits finishes, starting for each family at the related photon circular geodesic.

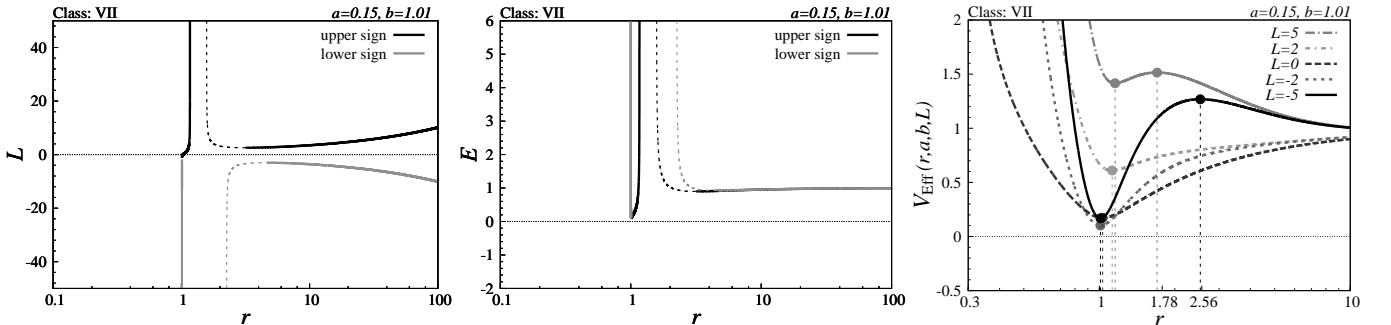


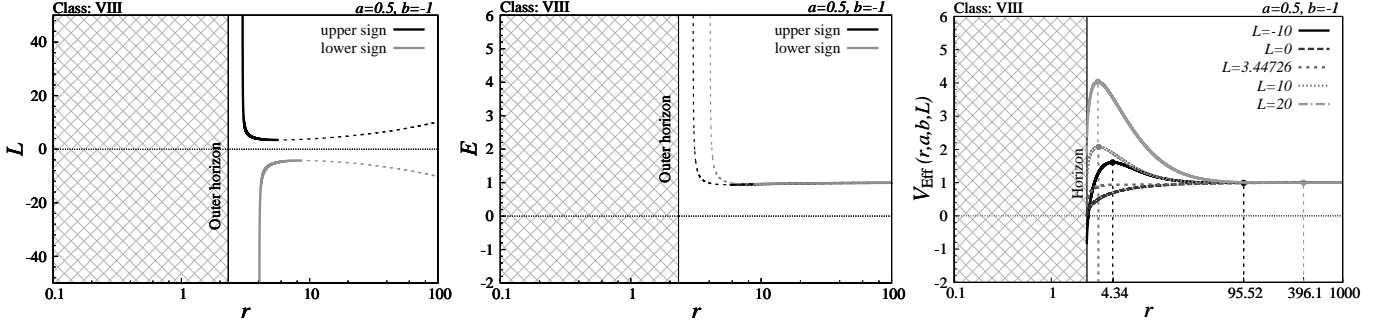
FIG. 21. L , E and effective potential for class VII.

12. Class VIII

Class of black hole spacetimes with negative braneworld tidal charge parameter b that has only one horizon located at $r > 0$, two unstable photon circular orbits and ergosphere. In the parameter space $b - a$, boundary of the region related to this class is given by

the line $b = -a^2$, and the line $a = 0$.

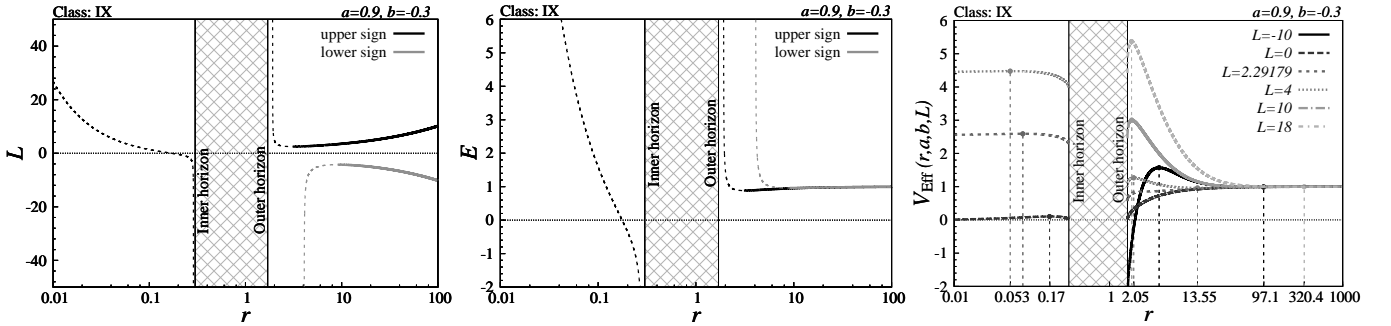
For both the lower and upper family circular geodesics the marginally stable orbit exist, determining the inner edge of the standard Keplerian disk. We obtained thus the standard situation typical for Kerr black holes, but no geodesic structure occurs at $r > 0$ under the event horizon.

FIG. 22. L , E and effective potential for class VIII.

13. Class IX

Class of black hole spacetimes with negative braneworld parameter b having two horizons, three unstable photon circular orbits and ergosphere. Border of the parameter space is given by the line $b = 1 - a^2$, line $b = -a^2$, and the line $b = 0$.

For both the lower and upper circular orbits the marginally stable orbit exists, giving in standard way the inner edge of the Keplerian accretion. Unstable orbits exist under the inner horizon.

FIG. 23. L , E and effective potential for class IX.

14. Class X

Class of naked singularity spacetimes with negative brane parameter b having one unstable photon circular orbit and ergosphere. Border of the related region of the parameter space is given by the line $b = 1 - a^2$,

and the line $b = 0$.

In these naked singularity spacetimes the marginally stable orbit exists for both the lower and upper family of circular geodesics, representing thus in both cases the inner edge of the Keplerian accretion disks. Under the marginally stable orbits only unstable orbits exist

for both families. From the point of view of the geodesic

structure, the naked singularity spacetimes of Class X resemble the standard Kerr naked singularity spacetimes.

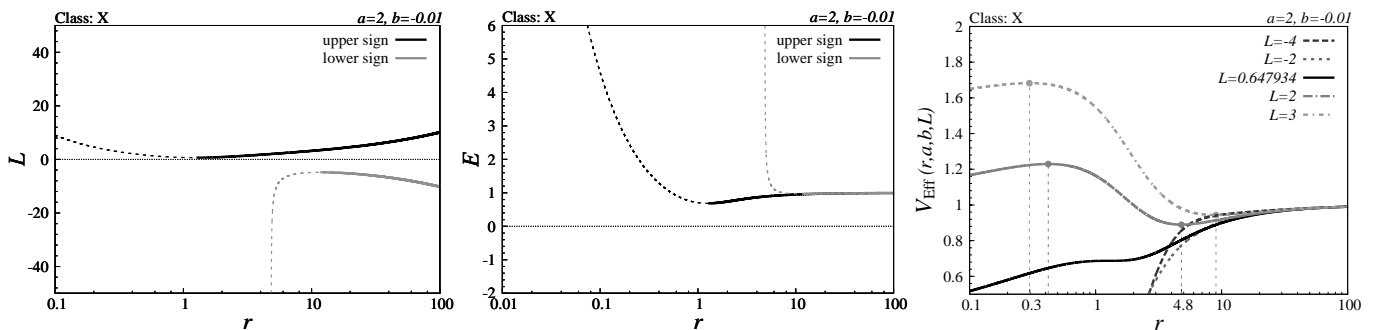


FIG. 24. L , E and effective potential for class X.

VII. EFFICIENCY OF THE KEPLERIAN ACCRETION

Now we are able to determine the energetic efficiency of the Keplerian accretion. From the astrophysical point of view, the standard Keplerian accretion is relevant in the regions enabling starting of accretion at large distance (infinity) and its finishing at the first inner edge that can be approached by a continuous accretion process. We determine efficiency of the Keplerian accretion for all the classes of the braneworld Kerr–Newman spacetimes for the standard Keplerian accretion. In some of these spacetimes there exists also an inner region where the Keplerian accretion could work due to the decline of both energy and angular momentum with decreasing radius. However, these regions are not related to the standard notion of Keplerian accretion and will not be considered here for calculations of the accretion efficiency. Moreover, there could exist also complexities of the Keplerian accretion process related to the behaviour of the angular velocity that are described in detail in [61] – we shall not discuss these subtleties in the present paper.

We concentrate our attention in determining the efficiency for the Keplerian accretion following the upper family circular geodesics, when the efficiency can be very high, being in some cases even unlimitedly high (formally). In the case of the upper family Keplerian accretion, the efficiency is discontinuous when transition between the naked singularity with sufficiently high dimensionless spin and the related extreme black hole state is considered. The critical value of the spin, and the related critical tidal charge reads

$$a_{\text{cr}} = \frac{1}{\sqrt{2}}, \quad b_{\text{cr}} = \frac{1}{2}. \quad (106)$$

We have to stress that the efficiency of the Keplerian accretion in the near-extreme naked singularity spacetimes exceeds significantly efficiency in the extreme black hole

spacetimes. On the other hand, the efficiency of the Keplerian accretion in the upper family regime is fully continuous in the case of transition of the naked singularity to extreme black hole spacetime with sufficiently low spin, $a < a_{\text{cr}}$, and for all the braneworld KN spacetimes in the case of the Keplerian accretion in the lower family accretion regime. Generally, the efficiency of the Keplerian accretion is substantially smaller in comparison to the upper family regime in a given Kerr–Newman spacetime.

The efficiency of the accretion for the geometrically thin Keplerian disks governed by the circular geodesics is defined by the relation

$$\eta(a, b) = 1 - E(r_{\text{edge}}, a, b), \quad (107)$$

where r_{edge} denotes location of the inner edge of the standard Keplerian accretion disks. For the Keplerian disks following the lower family circular geodesics, the inner edge of the disk is always located at the marginally stable geodesic giving thus always the scenario of the Keplerian accretion in the Kerr spacetimes. On the other hand, for the upper family Keplerian disks, the situation is more complex, as follows from the classification of the braneworld Kerr–Newman spacetimes. There can occur three qualitatively different cases in dependence on the combinations of dimensionless spacetime parameters a and b .

In the first family of classes of the Kerr–Newman spacetimes, the r_{edge} is simply located at the marginally stable geodesic, giving thus the scenario of the Keplerian accretion onto Kerr black holes – this case includes all the braneworld Kerr–Newman black hole spacetimes.

In the second family of the Kerr–Newman classes, the inner edge of the Keplerian disk is located at the radius $r = b$, giving thus the special case discovered at first for the Reissner–Nordström naked singularity spacetimes [15, 16]. In all classes with $b > 1$ (IV, V) the efficiency of the Keplerian accretion along the upper family of circular geodesics is independent of the spin parameter a being

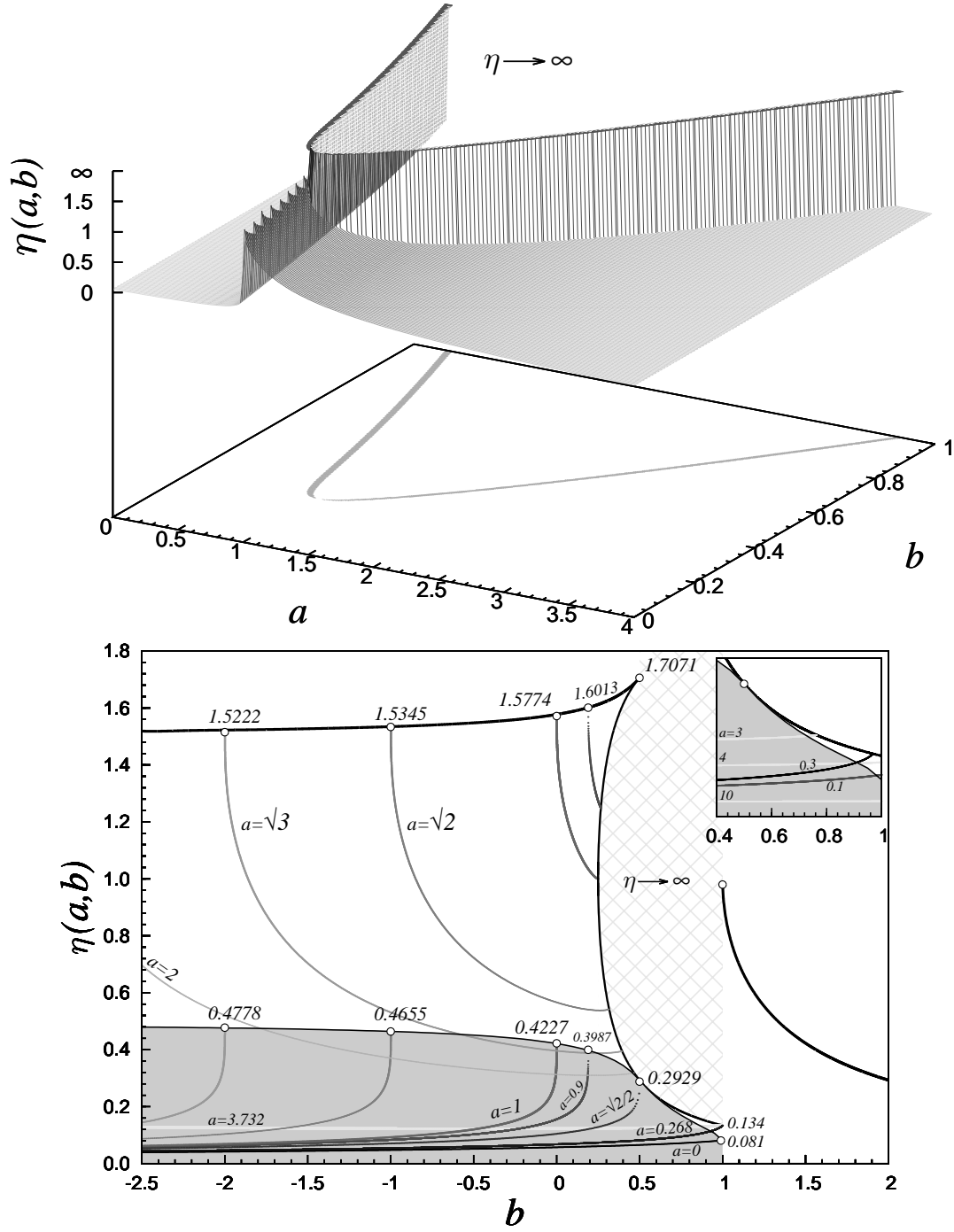


FIG. 25. Energetic efficiency $\eta(a, b)$ of the Keplerian accretion following the upper family circular geodesics is given in dependence on the spacetime dimensionless tidal charge parameter b and the spin parameter a . 3D diagram is reflecting the position of the special class of the mining unstable Kerr–Newman spacetimes of Class IIIa in the plane of the spacetime parameters. Due to a complex character of the efficiency function we give also the characteristic $a = \text{const}$ sections in the $\eta - b$ plane.

defined by the simple relation [69]

$$\eta(b) = 1 - \sqrt{1 - \frac{1}{b}}. \quad (108)$$

The efficiency goes slowly to 0% for $b \rightarrow \infty$ – see Figure (25).

In the third and most interesting family of the Kerr–Newman spacetime classes, r_{edge} corresponds to the radius of the stable photon orbit approached by particles with specific energy $E \rightarrow -\infty$ and specific angular momentum $L \rightarrow -\infty$ – notice that the limiting photon circular geodesic is a corotating one as the impact param-

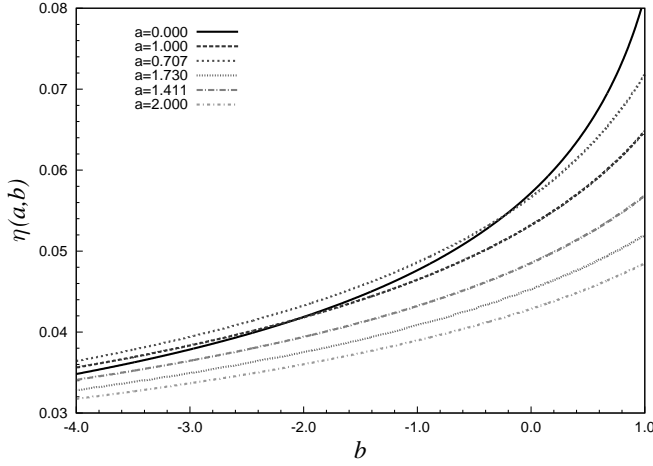


FIG. 26. Energy efficiency of the Keplerian accretion following the lower family circular geodesics is given in dependence on the spacetime dimensionless tidal charge parameter b for characteristic values of the spin parameter $a = \text{const}$.

eter $\lambda = L/E > 0$. In the third case, the Keplerian accretion efficiency approaches (theoretically) infinity. This effect occurs explicitly in the Class IIIa Kerr–Newman spacetimes as clearly demonstrated in Figure (11). For this class the tidal charge parameter $b \in (1/4, 1)$ and the dimensionless spin $a \in (2\sqrt{b} - \sqrt{b(4b-1)}, 2\sqrt{b} + \sqrt{b(4b-1)})$.

The Keplerian accretion efficiency is given for the upper family of circular geodesics in Figure 25, and for the lower family circular orbits in Figure 26. Because of its complexity, we represent the case of the upper family accretion regime by a 3D figure with addition of the figure representing the relevant sections $a = \text{const}$. In the case of the lower family accretion regime, the representative $a = \text{const}$ sections are sufficient to clearly demonstrate the character of the efficiency of the Keplerian accretion.

For the Keplerian accretion along the lower family circular geodesics the situation is quite simple and the efficiency is always continuously matched between the naked singularity and the extreme black hole states. The efficiency of the lower family regime accretion for fixed dimensionless spin a of the braneworld Kerr–Newman spacetimes always decreases with decreasing tidal charge parameter b . Moreover, for fixed tidal charge b , the efficiency decreases with increasing spin a .

In order to understand the upper family Keplerian accretion regime and its efficiency, the dependences $\eta(b, a = \text{const})$ are most instructive. They are governed by two crucial families of curves. First, the efficiency of the Keplerian accretion in the extreme braneworld KN black hole spacetimes, and the related near-extreme braneworld KN naked singularity spacetimes is given by the relation

$$\eta_{\text{jump}}(b) = 1 \pm \frac{1}{\sqrt{4 - \frac{1}{1-b}}}, \quad (109)$$

where the $+$ sign corresponds to the efficiency in the near-extreme naked singularity spacetimes, while the $-$ sign corresponds to the related extreme black holes. Naturally, this formula is relevant in the interval of the tidal charge $b \in (-\infty, 0.5)$, i.e., up to the critical value of the tidal charge. Second crucial curve is given by the efficiency of the accretion in the limiting spacetimes governed by the boundary of Class IIIa spacetimes, $\eta_{\text{mining}}(b, a_{\text{mining}\pm}(b))$, where $b \in (1/4, 1)$, and $a_{\text{mining}}(b) = 2\sqrt{b} \pm \sqrt{b(4b-1)}$.

The results can be summarized in the following way. For whole the braneworld spacetimes with the negative tidal charge parameter $b < 0$, and for those with positive charge parameter $0 \leq b \leq 1/2$, the large jump of the efficiency in transition between the +naked singularity to the related extreme black hole state occurs. Such a jump was observed for the first time in the case of transition between the Kerr naked singularity and the extreme Kerr black hole ($b = 0$) where $\eta \sim 1.57$ goes down to $\eta \sim 0.43$ [35]. For the braneworld KN extreme black holes (related near-extreme naked singularities), the efficiency slightly increases (decreases) with negatively valued tidal charge increasing in its magnitude, so the efficiency jump slightly decreases from its maximal Kerr value. On the other hand, for $b \in (0, 1/2)$, the efficiency for the extreme black holes (near-extreme naked singularities) decreases (increases), and the jump fastly increases – for $b = 1/2$, the efficiency jumps from $\eta \sim 1.707$ down to $\eta \sim 0.293$.

For the naked singularities with the tidal charge in the interval $1/4 < b < 1$, and the dimensionless spin in the interval $a \in (2\sqrt{b} - \sqrt{b(4b-1)}, 2\sqrt{b} + \sqrt{b(4b-1)})$ the formally defined efficiency of the Keplerian accretion is unlimited. At the boundary of this region, the efficiency is given by the limit governed by the regular Keplerian accretion finished at the marginally stable orbit.

For the naked singularities with $b < 1/2$, the efficiency of the Keplerian accretion, starting at the near-extreme state and keeping spin $a = \text{const}$, decreases with increasing tidal charge down to the curve $\eta_{\text{mining}}(b, a_{\text{mining}\pm}(b))$. Further increase of b causes entrance to the region of unlimited efficiency. The curve $\eta(b, a = 1)$ starts at $b = 0$ and finishes at $b = 1/4$, giving the related efficiency $\eta = 1$. For spin in the interval $1 > a > 1/\sqrt{2}$, the curves $\eta(b, a = 1)$ start at the extreme state and finish at the state with $0 < b < 1/2$ and efficiency $\eta > 1$. For spin approaching $a = 1/\sqrt{2}$, the curve $\eta(b, a = \text{const})$ degenerates at the point with $b = 1/2$, and efficiency approaching $\eta \sim 1.707$. For higher values of spin, $a \in (1, 2 + \sqrt{3})$, the efficiency curves $\eta(b, a = \text{const})$ decrease to the curve $\eta_{\text{mining}}(b, a_{\text{mining}\pm}(b))$ with b increasing in the interval $b \in (1/4, 1)$ and the efficiency decreasing down to the limiting value of $\eta(b = 1, a = 2 + \sqrt{3}) \sim 0.134$.

For tidal charge $b \in (1/2, 1)$, the efficiency of the Keplerian accretion at the transition between the extreme black hole and the related near-extreme naked singularity is continuously matched. The efficiency of $\eta \sim 0.134$

is reached for the Kerr–Newman spacetime with $b = 1$ and $a = 2 - \sqrt{3}$. For values of the spin in the interval of $a \in (2 - \sqrt{3}, 1/\sqrt{2})$, the transition of the function $\eta(b, a = \text{const})$ between the black hole and naked singularity states, obtained due to increasing tidal charge b , is still continuous, and the curve $\eta_{\text{mining}}(b, a_{\text{mining}\pm}(b))$ is reached at values $\eta < 0.293$.

With increasing spin a , the efficiency of the Keplerian accretion decreases. It is interesting that for naked singularities having spin a higher than ~ 4.97 and appropriately valued tidal charge b , the efficiency reaches values smaller than those corresponding to the Schwarzschild black holes ($\eta \sim 0.057$).

Note that the results of the Keplerian accretion analysis for the braneworld Kerr–Newman spacetimes can be directly applied also for the Keplerian accretion in the standard Kerr–Newman spacetimes, if we make transformation $b \rightarrow Q^2$ where Q^2 represent the electric charge parameter of the Kerr–Newman background.

VIII. CONCLUSIONS

In the present paper the circular geodesics of the braneworld Kerr–Newman black hole and naked singularity spacetimes have been studied and classification of these spacetimes according to character of the circular geodesic structure has been presented. The circular geodesics have been separated into two families – the lower family containing only the counterrotating circular geodesics, and the upper family with corotating geodesics at large distance, but possible transformation to counterrotating geodesics in vicinity of the naked singularity. It has been demonstrated that fourteen different classes of the Kerr–Newman spacetimes can exist, mainly due to the properties of the upper family of circular geodesics. Implications of the geodesic structure to the Keplerian accretion have been given, and efficiency of the Keplerian accretion have been determined. The accretion efficiency is continuously matched between the naked singularity and extreme black hole spacetimes for the Keplerian accretion along the lower family circular geodesics. On the other hand, there is a strong discontinuity occurring in the transition between the naked singularities and the extreme black holes for the Keplerian accretion along the upper family circular geodesic, if the dimensionless spin of the Kerr–Newman spacetime is sufficiently high ($a > 1/\sqrt{2}$) – the energy efficiency of the Keplerian accretion is then substantially higher for the naked singularity spacetimes. The accretion efficiency could then go up to the value of $\eta \sim 1.707$ for Kerr–Newman near-extreme naked singularity spacetimes with $b \sim 1/2$ and $a \sim 1/\sqrt{2}$.

For the Keplerian accretion along the lower family circular geodesics, the inner edge of the disk has to be always located at the marginally stable circular geodesic corresponding to an inflexion point of the effective potential of the motion in accord with the scenario of Keplerian

accretion onto Kerr black holes and naked singularities.

It has been shown that the Keplerian accretion along the upper family geodesics can give three different scenarios. It can finish at the inner edge located at the marginally stable circular geodesic – this is the standard accretion scenario present in the black hole spacetimes. However, two other scenarios could occur in the naked singularity spacetimes. The inner edge of the Keplerian accretion could occur at $r = b$ that is the special limit on existence of the circular geodesics. For $b > 1$ the efficiency of the upper family Keplerian accretion is independent of the naked singularity spin. The most interesting is the third scenario, related to the Kerr–Newman naked singularity spacetimes of Class IIIa having an infinitely deep gravitational potential of the upper family Keplerian accretion. Then the inner edge of the Keplerian accretion could occur even at the stable photon circular geodesic, and the accretion efficiency could be formally unlimited, making such naked singularity spacetimes unstable relative to accretion “mining”.

The mining instability of the Kerr–Newman naked singularity spacetimes (or related superspinars) is a classical instability that could imply interesting consequences that we plan to study in future. Nevertheless, it is clear that the mining instability have to be restricted at least by validity of the test particle approximation used in the present paper for the Keplerian accretion.

The other classical instability, related to the conversion of Kerr naked singularities to extreme black holes due to the Keplerian accretion [36], has to be treated in future work, but this instability has necessarily much more complex character in the Kerr–Newman naked singularity spacetimes in comparison to the relatively simple Kerr case, due to the complexities related to the mining instability and the influence of the tidal charge.

Interesting phenomena could be expected in the mining unstable Kerr–Newman spacetimes (Class IIIa) even if it will represent astrophysically more acceptable concept of Kerr–Newman superspinar, with the inner boundary of the Kerr–Newman spacetime located at least at the outer boundary of the causality violation region [37, 40, 41]. We can expect observations of extremely high energy coming out of collisions in vicinity of such an superspinar, enabled by non-existence of the event horizon and fast rotation of the superspinar, or inversely, strong magnification of incoming radiation [42, 66]. We could expect a hot doughnut-shaped configuration of accreting matter surrounding the superspinar, as discussed in [61].

ACKNOWLEDGEMENTS

ZS and MB has been supported by the Albert Einstein Centre for Gravitation and Astrophysics financed by the Czech Science Agency Grant No. 14-37086G and by the Silesian University at Opava grant SGS/14/2016. MB thanks Petr Slaný for several discussions.

-
- [1] P. Hořava and E. Witten. Eleven-dimensional supergravity on a manifold with boundary. *Nuclear Physics B*, 475:94–114, February 1996.
- [2] P. Hořava and E. Witten. Heterotic and Type I string dynamics from eleven dimensions. *Nuclear Physics B*, 460:506–524, February 1996.
- [3] N. Arkani-Hamed, S. Dimopoulos, and G. Dvali. The hierarchy problem and new dimensions at a millimeter. *Physics Letters B*, 429:263–272, June 1998.
- [4] L. Randall and R. Sundrum. An Alternative to Compactification. *Physical Review Letters*, 83:4690–4693, December 1999.
- [5] S. Dimopoulos and G. Landsberg. Black Holes at the Large Hadron Collider. *Physical Review Letters*, 87(16):161602, October 2001.
- [6] T. Shiromizu, K.-I. Maeda, and M. Sasaki. The Einstein equations on the 3-brane world. *Physical Review D*, 62(2):024012, July 2000.
- [7] C. Germani and R. Maartens. Stars in the braneworld. *Physical Review D*, 64(12):124010, December 2001.
- [8] J. Hladík and Z. Stuchlík. Photon and neutrino redshift in the field of braneworld compact stars. *Journal of Cosmology and Astroparticle Physics*, 7:012, July 2011.
- [9] Z. Stuchlík, J. Hladík, and M. Urbanec. Neutrino trapping in braneworld extremely compact stars. *General Relativity and Gravitation*, 43:3163–3190, November 2011.
- [10] N. Dadhich, R. Maartens, P. Papadopoulos, and V. Rezanian. Black holes on the brane. *Physics Letters B*, 487:1–6, August 2000.
- [11] A. N. Aliev and A. E. Gümrükçüoğlu. Charged rotating black holes on a 3-brane. *Physical Review D*, 71(10):104027, May 2005.
- [12] C. W. Misner, K. S. Thorne, and J. A. Wheeler. *Gravitation*. 1973.
- [13] Z. Stuchlík and M. Calvani. Null geodesics in black hole metrics with non-zero cosmological constant. *General Relativity and Gravitation*, 23:507–519, May 1991.
- [14] Z. Stuchlík and S. Hledík. Equatorial photon motion in the Kerr-Newman spacetimes with a non-zero cosmological constant. *Classical and Quantum Gravity*, 17:4541–4576, November 2000.
- [15] Z. Stuchlík and S. Hledík. Properties of the Reissner-Nordström Spacetimes with a Nonzero Cosmological Constant. *Acta Physica Slovaca*, 52(5):363–407, oct 2002.
- [16] D. Pugliese, H. Quevedo, and R. Ruffini. Equatorial circular motion in Kerr spacetime. *Physical Review D*, 84(4):044030, August 2011.
- [17] D. Pugliese, H. Quevedo, and R. Ruffini. Equatorial circular orbits of neutral test particles in the Kerr-Newman spacetime. *Physical Review D*, 88(2):024042, July 2013.
- [18] J. Schee and Z. Stuchlík. Profiles of emission lines generated by rings orbiting braneworld Kerr black holes. *General Relativity and Gravitation*, 41:1795–1818, August 2009.
- [19] J. Schee and Z. Stuchlík. Optical Phenomena in the Field of Braneworld Kerr Black Holes. *International Journal of Modern Physics D*, 18:983–1024, 2009.
- [20] A. Y. Bin-Nun. Relativistic images in Randall-Sundrum II braneworld lensing. *Physical Review D*, 81(12):123011, June 2010.
- [21] E. F. Eiroa. Braneworld black hole gravitational lens: Strong field limit analysis. *Physical Review D*, 71(8):083010, April 2005.
- [22] F. Atamurotov, A. Abdujabbarov, and B. Ahmedov. Shadow of rotating non-Kerr black hole. *Physical Review D*, 88(6):064004, September 2013.
- [23] J. Jiang, C. Bambi, and J. F. Steiner. Testing the Kerr nature of black hole candidates using iron line reverberation mapping in the Cardoso-Pani-Rico framework. *Physical Review D*, 93(12):123008, June 2016.
- [24] D. Liu, Z. Li, and C. Bambi. Testing a class of non-Kerr metrics with hot spots orbiting SgrA*. *Journal of Cosmology and Astroparticle Physics*, 1:020, January 2015.
- [25] Z. Li, L. Kong, and C. Bambi. Testing the Nature of the Supermassive Black Hole Candidate in SgrA* with Light Curves and Images of Hot Spots. *The Astrophysical Journal*, 787:152, June 2014.
- [26] C. G. Böhrmer, T. Harko, and F. S. N. Lobo. Solar system tests of brane world models. *Classical and Quantum Gravity*, 25(4):045015, February 2008.
- [27] A. Kotrllová, Z. Stuchlík, and G. Török. Quasiperiodic oscillations in a strong gravitational field around neutron stars testing braneworld models. *Classical and Quantum Gravity*, 25(22):225016, November 2008.
- [28] Z. Stuchlík and A. Kotrllová. Orbital resonances in discs around braneworld Kerr black holes. *General Relativity and Gravitation*, 41:1305–1343, June 2009.
- [29] A. N. Aliev and P. Talazan. Gravitational effects of rotating braneworld black holes. *Physical Review D*, 80(4):044023, August 2009.
- [30] A. Abdujabbarov and B. Ahmedov. Test particle motion around a black hole in a braneworld. *Physical Review D*, 81(4):044022, February 2010.
- [31] O. G. Rahimov, A. A. Abdujabbarov, and B. J. Ahmedov. Magnetized particle capture cross section for braneworld black hole. *Astrophysics and Space Science*, 335:499–504, October 2011.
- [32] V. S. Morozova and B. J. Ahmedov. Electromagnetic fields of slowly rotating compact magnetized stars in braneworld. *Astrophysics and Space Science*, 333:133–142, May 2011.
- [33] S. R. Shaymatov, B. J. Ahmedov, and A. A. Abdujabbarov. Particle acceleration near a rotating black hole in a Randall-Sundrum brane with a cosmological constant. *Physical Review D*, 88(2):024016, July 2013.
- [34] F. de Felice. Repulsive Phenomena and Energy Emission in the Field of a Naked Singularity. *Astronomy and Astrophysics*, 34:15, August 1974.
- [35] Z. Stuchlík. Equatorial circular orbits and the motion of the shell of dust in the field of a rotating naked singularity. *Bulletin of the Astronomical Institutes of Czechoslovakia*, 31:129–144, 1980.
- [36] Z. Stuchlík, S. Hledík, and K. Truparová. Evolution of Kerr superspinars due to accretion counterrotating thin discs. *Classical and Quantum Gravity*, 28(15):155017, August 2011.
- [37] Z. Stuchlík and J. Schee. Observational phenomena related to primordial Kerr superspinars. *Classical and Quantum Gravity*, 29(6):065002, March 2012.
- [38] R. C. Henry. Kretschmann Scalar for a Kerr-Newman Black Hole. *The Astrophysical Journal*, 535:350–353,

- May 2000.
- [39] B. Carter. Black hole equilibrium states. In C. Dewitt and B. S. Dewitt, editors, *Black Holes (Les Astres Occlus)*, pages 57–214, 1973.
 - [40] E. G. Gimon and P. Hořava. Astrophysical violations of the Kerr bound as a possible signature of string theory. *Physics Letters B*, 672:299–302, February 2009.
 - [41] Z. Stuchlík and J. Schee. Appearance of Keplerian discs orbiting Kerr superspinars. *Classical and Quantum Gravity*, 27(21):215017, November 2010.
 - [42] Z. Stuchlík and J. Schee. Ultra-high-energy collisions in the superspinning Kerr geometry. *Classical and Quantum Gravity*, 30(7):075012, April 2013.
 - [43] J. M. Bardeen, W. H. Press, and S. A. Teukolsky. Rotating Black Holes: Locally Nonrotating Frames, Energy Extraction, and Scalar Synchrotron Radiation. *Astrophysical Journal*, 178:347–370, December 1972.
 - [44] Z. Stuchlík, J. Bičák, and V. Bálek. The Shell of Incoherent Charged Matter Falling onto a Charged Rotating Black Hole. *General Relativity and Gravitation*, 31:53–71, January 1999.
 - [45] B. Carter. Global Structure of the Kerr Family of Gravitational Fields. *Physical Review*, 174:1559–1571, October 1968.
 - [46] G. V. Kraniotis. Frame dragging and bending of light in Kerr and Kerr (anti) de Sitter spacetimes. *Classical and Quantum Gravity*, 22:4391–4424, November 2005.
 - [47] G. V. Kraniotis. Periastron and gravitomagnetic precessions of stellar orbits in Kerr and Kerr de Sitter black hole spacetimes. *Classical and Quantum Gravity*, 24:1775–1808, April 2007.
 - [48] Z. Stuchlík. The motion of test particles in black-hole backgrounds with non-zero cosmological constant. *Bulletin of the Astronomical Institutes of Czechoslovakia*, 34:129–149, March 1983.
 - [49] Z. Stuchlík and S. Hledík. Some properties of the Schwarzschild-de Sitter and Schwarzschild-anti-de Sitter spacetimes. *Physical Review D*, 60(4):044006, August 1999.
 - [50] G. V. Kraniotis. Gravitational lensing and frame dragging of light in the Kerr-Newman and the Kerr-Newman (anti) de Sitter black hole spacetimes. *General Relativity and Gravitation*, 46:1818, November 2014.
 - [51] Z. Stuchlík. Evolution of Kerr naked singularities. *Bulletin of the Astronomical Institutes of Czechoslovakia*, 32:68–72, 1981.
 - [52] V. Bálek, J. Bičák, and Z. Stuchlík. The motion of the charged particles in the field of rotating charged black holes and naked singularities. II - The motion in the equatorial plane. *Bulletin of the Astronomical Institutes of Czechoslovakia*, 40:133–165, June 1989.
 - [53] S. Hledík and Z. Stuchlík, editors. *RAGtime 8/9: Workshops on black holes and neutron stars*, December 2007.
 - [54] Z. Kovács and T. Harko. Can accretion disk properties observationally distinguish black holes from naked singularities? *Physical Review D*, 82(12):124047, December 2010.
 - [55] N. Dadhich and P. P. Kale. Equatorial circular geodesics in the Kerr-Newman geometry. *Journal of Mathematical Physics*, 18:1727–1728, 1977.
 - [56] I. D. Novikov and K. S. Thorne. Astrophysics of black holes. In C. Dewitt and B. S. Dewitt, editors, *Black Holes (Les Astres Occlus)*, pages 343–450, 1973.
 - [57] D. N. Page and K. S. Thorne. Disk-Accretion onto a Black Hole. Time-Averaged Structure of Accretion Disk. *Astrophysical Journal*, 191:499–506, July 1974.
 - [58] J. Bičák, Z. Stuchlík, and V. Bálek. The motion of charged particles in the field of rotating charged black holes and naked singularities. *Bulletin of the Astronomical Institutes of Czechoslovakia*, 40:65–92, March 1989.
 - [59] J. M. Bardeen. Timelike and null geodesics in the Kerr metric. In C. Dewitt and B. S. Dewitt, editors, *Black Holes (Les Astres Occlus)*, pages 215–239, 1973.
 - [60] R. Ruffini. On the energetics of black holes. In C. Dewitt and B. S. Dewitt, editors, *Black Holes (Les Astres Occlus)*, pages 451–546, 1973.
 - [61] Z. Stuchlík and J. Schee. Optical effects related to Keplerian discs orbiting Kehagias-Sfetsos naked singularities. *Classical and Quantum Gravity*, 31(19):195013, October 2014.
 - [62] J. Bičák and Z. Stuchlík. On the latitudinal and radial motion in the field of a rotating black hole. *Bulletin of the Astronomical Institutes of Czechoslovakia*, 27:129–133, 1976.
 - [63] Formally same results relevant for Kerr–Newman space-time can be found in [70].
 - [64] See for example [15, 71].
 - [65] Z. Stuchlík. Null geodesics in the Kerr-Newman metric. *Bulletin of the Astronomical Institutes of Czechoslovakia*, 32:366–373, 1981.
 - [66] Z. Stuchlík, J. Schee, and A. Abdurjabbarov. Ultra-high-energy collisions of particles in the field of near-extreme Kehagias-Sfetsos naked singularities and their appearance to distant observers. *Physical Review D*, 89(10):104048, May 2014.
 - [67] Z. Stuchlík and J. Schee. Circular geodesic of Bardeen and Ayon-Beato-Garcia regular black-hole and no-horizon spacetimes. *International Journal of Modern Physics D*, 24:1550020–289, December 2015.
 - [68] J. Schee and Z. Stuchlík. Gravitational lensing and ghost images in the regular Bardeen no-horizon spacetimes. *Journal of Cosmology and Astroparticle Physics*, 6:048, June 2015.
 - [69] Interestingly, the Keplerian efficiency relation for the lower family of geodesics is much more complex and depends on the spin parameter a .
 - [70] A. N. Aliev and D. V. Galtsov. Radiation from relativistic particles in nongeodesic motion in a strong gravitational field. *General Relativity and Gravitation*, 13:899–912, October 1981.
 - [71] M. Favata. Conservative corrections to the innermost stable circular orbit (ISCO) of a Kerr black hole: A new gauge-invariant post-Newtonian ISCO condition, and the ISCO shift due to test-particle spin and the gravitational self-force. *Physical Review D*, 83(2):024028, January 2011.